Journal of Applied Physics

Voltage–current characteristics of low-pressure discharges in vapors of several alcohols

Cite as: J. Appl. Phys. **129**, 143303 (2021); https://doi.org/10.1063/5.0044419
Submitted: 15 January 2021 . Accepted: 26 March 2021 . Published Online: 12 April 2021

Jelena Marjanović, Dragana Marić, Gordana Malović, and Zoran Lj. Petrović

Journal of Applied Physics ARTICLE scitation.org/journal/jap

Voltage–current characteristics of low-pressure discharges in vapors of several alcohols

Cite as: J. Appl. Phys. **129**, 143303 (2021); doi: 10.1063/5.0044419
Submitted: 15 January 2021 · Accepted: 26 March 2021 ·
Published Online: 12 April 2021

Jelena Marjanović,[1] Dragana Marić,[1] Gordana Malović,[1] and Zoran Lj. Petrović[2,3,a)]

AFFILIATIONS

[1]Institute of Physics Belgrade, University of Belgrade, Pregrevica 118, 11080 Belgrade, Serbia
[2]School of Engineering, Ulster University, Jordanstown, County Antrim BT37 0QB, United Kingdom
[3]Serbian Academy for Sciences and Arts, Knez Mihailova 35, 11001 Belgrade, Serbia

Note: This paper is part of the Special Topic on Plasma-Liquid Interactions.
[a)]Author to whom correspondence should be addressed: z.petrovic@ulster.ac.uk

ABSTRACT

In this paper, we present the results for voltage–current (V–i) characteristics of dc low-pressure low to moderate current discharges in vapors of alcohols: methanol, ethanol, isopropanol, and n-butanol vapors. These electrical measurements are supported by optical recordings of axial emission profiles from low-current to high-current regimes. The voltage–current characteristics and the corresponding distribution of emission intensities were typically recorded for two pd values, in the left-hand branch of the Paschen curve (0.15 Torr cm) and in the minimum of the Paschen curves (ranging from 0.30 to 0.40 Torr cm for different alcohols selected here). In the recorded V–i characteristics, the different discharge regimes of discharge operation are easily distinguished. Axial profiles of emitted light from the low-current to high-current regimes reveal that heavy particles make up a significant contribution to excitation part in alcohol vapor discharges. In the region of transition from normal to abnormal glow in the methanol vapor discharge, sudden changes of the regime of operation were observed and several diagnostic techniques have been applied to them.

I. INTRODUCTION

Plasmas that operate in liquids and close to the gas–liquid interface have received a lot of attention in the past ten years.[1] First, they have a wide range of applications for nanoparticle synthesis, organic compound decomposition, sterilization, water treatment, etc., all the way to biomedical applications even including medical procedures. In addition to discharges associated with liquid water and its vapor, for several years, there has been an increasing interest in non-equilibrium discharges in alcohols and their vapors. Fast development of technology and industry imposes the need for such studies both from the fundamental point of view (elementary data, understanding of the main processes and phenomenology, the ability to represent transport in the presence of polar molecules, etc.) and also having in mind targeted applications where the most important examples are production of environmentally responsible fuels and production of pure carbon-based nanostructures.[2–7]

It is widely believed that in the future, hydrogen will have a major role as an energy carrier, much more than it is today. Alcohols have proven to be particularly attractive and suitable for hydrogen production using low-temperature non-equilibrium plasmas,[2,8,9] and they are used, for example, in the development of direct alcohol fuel cells (Proton Exchange Membrane Fuel Cells - PEMFC).[10–12] This sequence of technologies makes it possible to have production of fuel from the plants and, thus, achieve the most eco-friendly sustainable energy production and eventually consumption. Besides that, plasmas in alcohols are a good source of carbon and can be used for nanographene and nanotubes production.[3–7] A significant number of applications of these non-equilibrium discharges use sources of complicated electrode geometry. Those sources operate either in high-current discharge regimes or in a pulsed or a high-frequency glow regime. Therefore, unraveling all processes taking place in the discharge is an exacting task.

A long-term interest for elementary collision and transport data in alcohol vapors originated from the development of elementary particle detectors.[13–17] The development of new applications demands the availability of a sufficient range and depth of data and of understanding of the phenomenology that are well tested by

quantitative comparisons with experiments. These data can be obtained from studies of non-equilibrium discharges either directly motivated by a very specific application or in quite generic experiments with a simple electrode geometry. Therefore, our measurements of voltage-current characteristics in addition to the Paschen curves and emission profiles in non-equilibrium parallel-plate dc discharges in different alcohol vapors[18] aim at providing a comprehensive reference set of data that can be used in interpreting and modeling more complex discharges.[16,19–24] Our investigation follows similar steps as our previous studies of discharges in water vapor and in argon.[25,26]

It has been shown previously[27–29] that Paschen curves provide only a limited understanding of the breakdown itself or, in particular, of the secondary electron yields.[27,29–32] As it was predicted by phenomenological and physical theories as well as by simulations, a three-dimensional breakdown mapping consisting of V_b, pd, and jd^2 (where V_b is the breakdown voltage, p is the pressure, d is the gap in parallel-plate geometry, and j is the current density) is required for a complete description of the low-current discharge.[26,33] Here, in Fig. 1, we show one example (for methanol) of such 3D mapping of V_b, pd, and i characteristics. Note that the characteristics are presented as a function of the discharge current i, instead of jd^2, which is the proper scaling. The main point in Fig. 1 is that voltage–current characteristics are equally important in the analysis of the secondary electron yields as the Paschen curve.

Voltage–current characteristics (on their own or with support of other diagnostic techniques such as time-resolved fast intensified charge-coupled device (ICCD) recording of the variation in the discharge profile, observations of the presence of oscillations, and others) have been shown to be a valuable source of information on the energy (i.e., E/N) dependence of the secondary electron yields[26,29,31,34] in the presence of different modes of oscillations[31,35] and in the transitions between different modes of operation of low and moderate current discharges. In particular, modeling of the low-current diffuse Townsend regime may be used to determine a wide range of atomic and molecular collision data and understand relative contributions of different processes. Thus, we extend our initial work in establishing breakdown voltages (i.e., Paschen curves)[18] by determining voltage–current characteristics to discern which dominant species partake in the breakdown and in initialization of the non-equilibrium plasma under those circumstances.[36] Preliminary results for ethanol vapor, along such line of research, have been published in Ref. 37. In this paper, we extend our investigations to a wider range of conditions and to vapors of alcohols of different complexities.

The next step would be to apply all the theoretical/simulation tools in a similar fashion to what has been done for water vapor. Such modeling of well-defined experimental data may provide us with information on the most important processes and on the basic physical foundation of low-temperature plasmas in water and alcohol vapors.

While there have been several published studies of either breakdown voltage V_b vs pd (Paschen curves) or voltage–current characteristics of gas discharges, especially in the glow and dark Townsend regimes, we are not aware of any of such studies for alcohol vapors. With an improved theoretical understanding and a broader range of the available data, this study is also well motivated by the need to produce a basis for a more comprehensive data set for pertinent processes and by the need to address possible applications (as listed here) by detailed modeling.

This paper is an attempt to extend the existing studies in alcohol vapors (see Refs. 24 and 38–43) with a careful and well-defined procedure to measure the observables from the discharges in order to obtain some data on primary and secondary processes in a subsequent analysis.

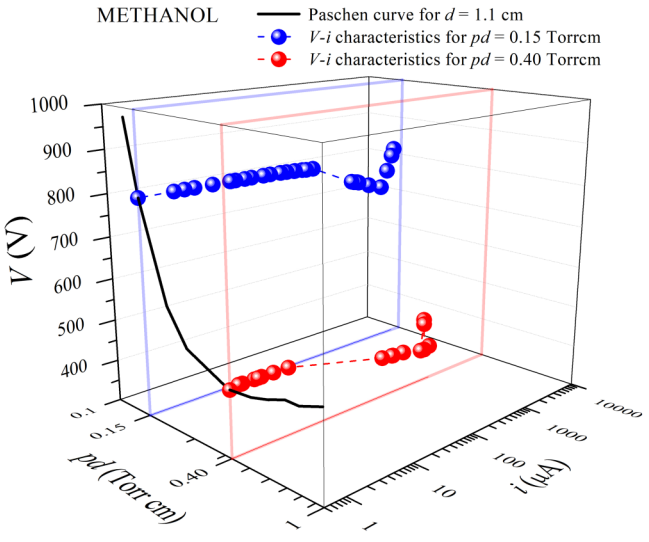

FIG. 1. V_b, pd, and i characteristics in the methanol vapor discharge for an electrode gap of 1.1 cm. The Paschen curve for the discharge in methanol vapor has been presented in our earlier paper,[18] while V–i characteristics for pd = 0.15 and 0.40 Torr cm are shown in the present paper in Fig. 3. The results presented here have been obtained by the experimental setup that will be described later in the present paper, and has been described elsewhere as well.[25,36]

II. EXPERIMENTAL SETUP

The schematic of the experimental setup (as described in previous papers[25,36,37,44]) is shown in Fig. 2. The discharge chamber consists of parallel plane electrodes placed inside a tightly fitting quartz tube. Each of the electrodes is 5.4 cm in diameter ($2r$). The cathode (C) is made of copper, and the anode (A) is made of quartz covered by a thin, transparent, conductive platinum film. This arrangement allows us to observe the radial profile of the discharge, constrictions, and diffuse regimes. The distance (d) between electrodes can be adjusted by fixed electrode supports, and for this experiment, it was set to 1.1 cm.

To obtain reproducible results, it is necessary to perform preparations before every measurement. Initially, the system is pumped down to an initial pressure of the order of 10^{-6} Torr. Before the measurements, the cathode surface is conditioned in a hydrogen discharge with a current around 30 μA (for approximately 40 min) until the operating voltage is stabilized. Hydrogen is chosen

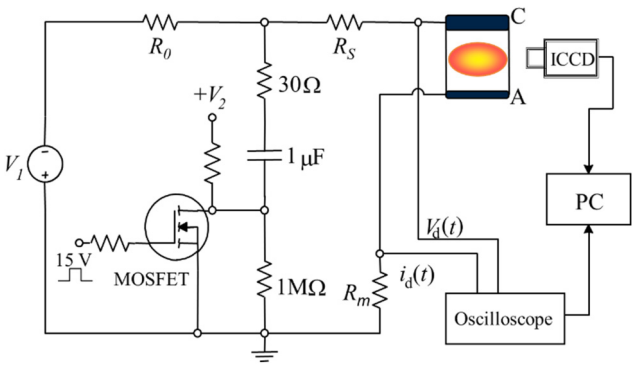

FIG. 2. Schematic of the experimental setup and the electrical circuit used in measurements.[25,36]

because it is lightweight; therefore, no cathode material is dispersed, and yet, it has the potential to remove oxide layers and react with organic vapors. At the same time, this treatment effectively removes chemical oxides and adsorbed layers of impurities from the cathode surface and, thus, produces the same surface conditions for each measurement. After cleaning of the cathode, the discharge chamber is again vacuumed to the pressure of around 10^{-6} Torr before the flow of gas is introduced. Both treatment with hydrogen discharge and measurements in alcohol vapors are done in a slow flow regime to ensure that possible impurities formed in the discharge chamber are continuously removed and kept at low abundance. Most importantly, our setup allows us to operate in a pulsed regime whereby current is maintained in a short period of time, sufficient to make measurement but too short so that damage to the cathode (due to sputtering) is avoided.[26,45,46]

We have performed measurements for four alcohols: methanol, ethanol, isopropanol (2-propanol), and *n*-butanol. The vapors are obtained from 99.5% purity methanol, isopropanol, and *n*-butanol and 95% purity ethanol (see our earlier papers[18,37]). For all the used alcohols in our measurements, water represents the most abundant declared impurity (max. 0.2%), while other volatile impurities such as acetone, aldehydes, and formic acid (max. 0.002%) are present in smaller quantities. Also, only in traces, there is iron (0.0005%) and some non-volatile substances (<0.001%). Therefore, a small percentage of water vapor may be present in the discharge. The presence of inherent gas impurities can be critical in two cases: the existence of significant vibrational energy losses introduced by molecular impurities in rare gases (this can strongly affect the breakdown data in atomic gases as molecular impurities introduce significant energy losses below the threshold for electronic excitations) and in the occurrence of the attachment to impurities. However, neither of the two is expected to strongly affect the results for gas discharges where ionization is the key process and is dominated by the most abundant gas. Therefore, water will not affect the results strongly through either of the two mentioned mechanisms and the same is true for all other listed components.

The vapor is introduced into the chamber at low pressure from a container with a liquid sample through a pressure regulatory valve at a low flow rate. Immediately after opening the valve, alcohol begins to boil due to the pressure difference above the surface and partial pressure of gases dissolved in the sample. Throughout this process, alcohol becomes devoid of dissolved volatile constituents, and after a few seconds, the sample surface becomes still. After that, the vapor is maintained at a moderate pressure (lower than the vapor pressure) in the chamber for periods of 1–2 h to saturate the electrodes and the chamber walls. The vapor pressures of methanol, ethanol, isopropanol, and *n*-butanol at room temperature (25 °C) are around 127, 45, 44, and 7 Torr, respectively;[47] therefore, during the measurements, operating pressures are kept well below these values to avoid formation of liquid droplets.

Our electrical circuit allows a current pulse of desired length and amplitude to be superimposed onto a dc discharge running at a very low current (typically around 1 μA) to avoid breakdown delays.[26,44] Pulse duration is long enough so that a steady-state discharge is developed and also sufficient to make reliable recordings. In this way, by minimizing gas heating and cathode heating and conditioning,[44,48] results of measurements of voltage–current characteristics (V–i) are stable and reproducible. Construction of the chamber allows recording of axial discharge profiles using a sensitive ICCD (Andor IStar DH720-18U-03). For spectrally resolved measurements of a spatial distribution of emission intensity, we used a bandpass optical filter in front of the lens, which enabled recordings of emission profiles for a CH band at 431.2 nm.

III. RESULTS AND DISCUSSION

A. Voltage–current characteristics

In Fig. 3, we show voltage–current characteristics of low to moderate current discharges in four alcohol vapors: methanol, ethanol, isopropanol, and *n*-butanol recorded at electrode distances of 1.1 cm for two *pd* values. The results obtained for different combinations of resistors R_s and R_m are represented by different symbols. The voltage is represented at the y axis by ΔV as the difference between the discharge voltage V and the breakdown voltage V_b. This way of the result presentation eliminates small differences in breakdown voltages in different sets of measured data, which does not affect the "dynamic" voltage–current characteristics.[48,49] At the same time, presenting the difference in voltage before and after the breakdown makes it possible to show small changes in the voltage that would be otherwise too small to observe on top of a large breakdown voltage.

The recorded voltage–current characteristics clearly show the areas of different operating modes through which the discharge passes with an increase of the current: Townsend discharge (low-current discharge), normal glow discharge, and abnormal glow discharge [in Fig. 3, the operating regimes are marked in graphs with letters (a)–(c), respectively].[36] The break in the voltage–current characteristics matches the area of free running, undamped oscillations. This area expands with an increase in the gas pressure. It can be seen that the abnormal discharge regime has a higher slope at higher pressures for all alcohol vapors presented here. This is in

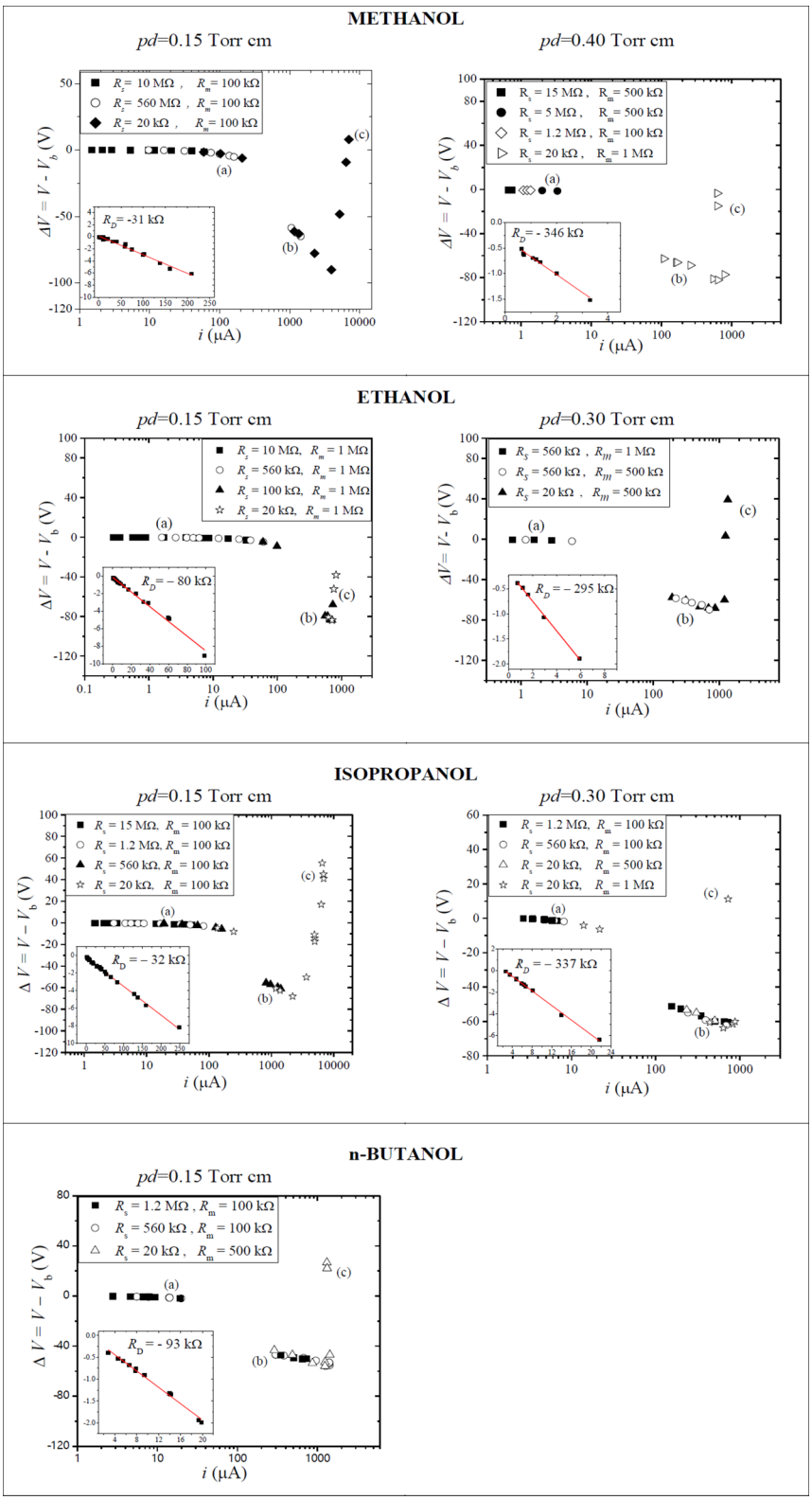

FIG. 3. Voltage–current characteristics for low-pressure dc discharges in alcohol vapors recorded at $d = 1.1$ cm at different pd values: in the left-hand branch of Paschen curve—$pd = 0.15$ Torr cm and at the minimum of the Paschen curves—$pd = 0.40$ and 0.30 Torr cm. V is the discharge voltage, while V_b denotes the breakdown voltage. Inserted graphs show negative differential resistance R_D that is obtained in our experiment for the steady-state Townsend regime.

contrast with the water vapor where higher slopes have been recorded at lower pressures.[25]

The negative differential resistance R_D at the lowest currents is determined for the steady-state (or dark) Townsend regime, and it has been determined by fitting the low-current portion of the measured voltage–current characteristics (the fits and the results are presented in the inserted graphs of Fig. 3). In other words, the negative slope of the Townsend discharge area [in Fig. 3 marked with the letter (a) on the graphs] corresponds to negative differential resistance. Negative differential resistance is a consequence of the spatial charge effects that occur due to the increase of the discharge current,[31,45] as well as the dependence of the secondary electron emission on the current and discharge voltage. A positive spatial charge effectively increases the electric field in front of the cathode, thereby exponentially increasing the ionization coefficient and the secondary electron yield, allowing the stable operation of the discharge at a lower voltage. Thus, an increase in the concentration of the spatial charge leads to inhomogeneity of the field, which in turn causes a decrease in the discharge voltage.

Simultaneously with measurements of voltage and current, i.e., V–i characteristics, we recorded corresponding spatial distributions of light emission from discharge, which were used to obtain axial profiles of emission (Fig. 4). At this point, we try to illustrate different regimes. A more thorough representation of spatial profiles will be presented when we develop a complete modeling set that would provide contributions of different high energy particles to emission and consequently their role in the breakdown. These recordings include spatial profiles of the total emission in a visual spectral range and a spatial distribution of emission in a narrow wavelength interval around the most intense lines in the visible part of the spectrum (for the CH band at 431.2 nm).

In Fig. 4, we show examples of spatial emission profiles at two pd values (0.15 and 0.40 Torr cm) in the methanol vapor discharge that indicate how emission profiles may be used for the identification of the discharge operation regime, and from additional information and modeling, one may identify the pertinent physical agents that contribute to the discharge under those conditions.

From the axial emission profiles obtained for pd = 0.15 Torr cm [Fig. 4(I)] in the methanol vapor discharge in all

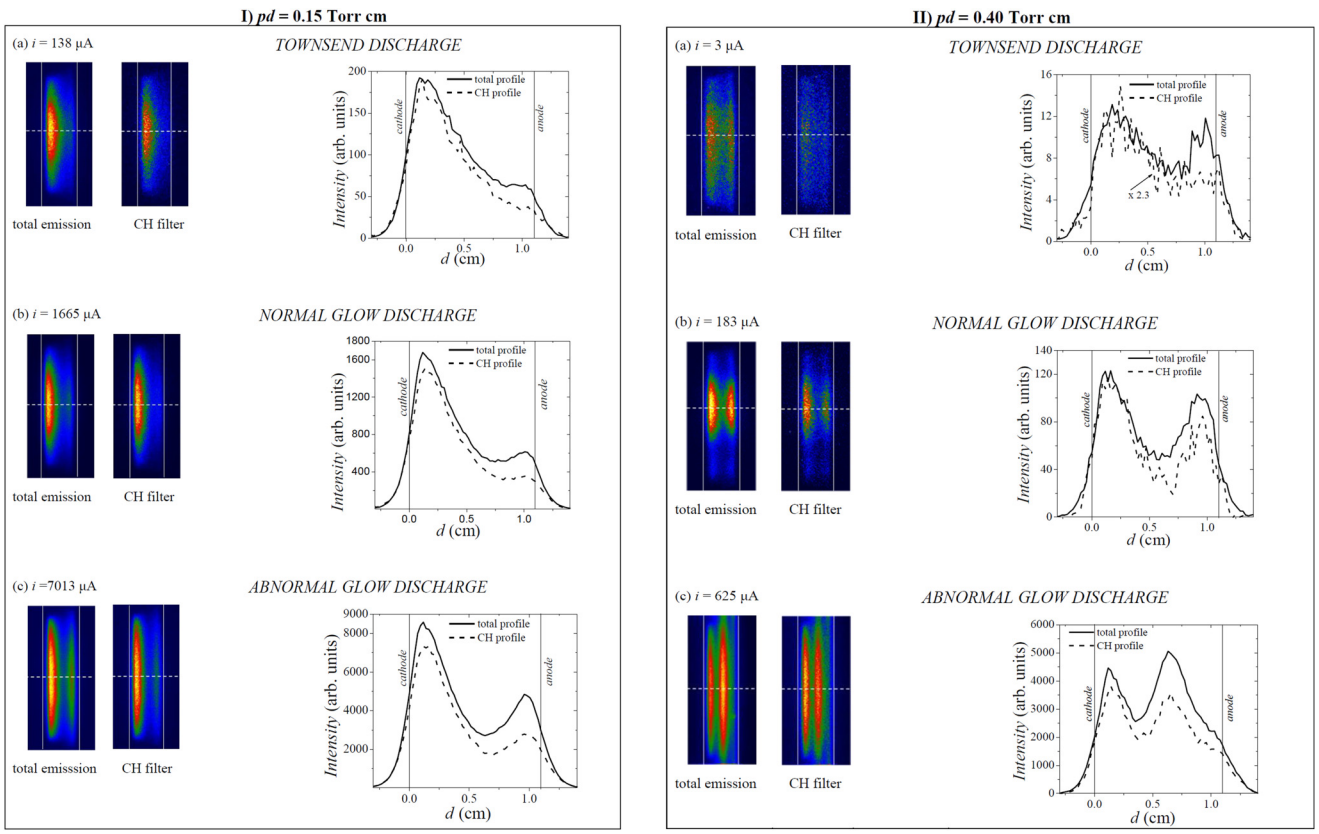

FIG. 4. Axial profiles of emission for discharges in methanol vapor for (I) pd = 0.15 Torr cm and (II) 0.40 Torr cm, obtained along with the recording of voltage–current characteristics at d = 1.1 cm, that correspond to different regimes marked with letters (a)–(c) in Fig. 3. The CH profile of Townsend emission at pd = 0.40 Torr cm was multiplied with a factor of 2.3 for easier comparison with a profile of total emission in the visible spectrum.

regimes, processes induced by heavy particles play a major role in excitation and ionization of gas/vapor, which is revealed in the existence of the peak of intensity in front of the cathode.[50,51] Also, the CH profile (dashed line) follows the shape of the total profile (solid line). With increasing current, the contribution of electron processes increases in discharge—the noticeable higher peak of intensity in front of the anode [Figs. 4(I) (b) and 4(I) (c)]. In all regimes, the CH profile (dashed line) has a maximum peak in front of the cathode.

At higher pressure, at *pd* that corresponds to the minimum of the Paschen curve for the methanol vapor discharge [*pd* = 0.40 Torr cm, Fig. 4(II)], the processes induced by heavy particles and electrons have almost equal contributions in excitation—maximum intensities of emission in front electrodes are approximately equal (solid line) [Fig. 4(II) (a)].

Electrons are accelerated toward the anode and they multiply followed by an exponentially rising emission profile as the equilibration of electrons is rather fast. The ions produced in ionizations move toward the cathode gaining energy. The growth of the ion density and the related emission profile are not exponential, but the density peaks by the cathode. It has been assumed in the past that these ions produce excitation in collisions with gas molecules, but due to the shape of their cross sections, ions begin to contribute only at very high energies.[51–55] At energy characteristics of the ions in standard Townsend discharges, the excitation peaking toward the cathode was shown to be due to fast neutrals produced from the fast ions in charge exchange collisions. Such collisions leave ions standing still, while neutrals leave the collision with close to the full energy of the projectile ion. Fast neutrals may also reflect from the cathode and move toward the anode, thus giving two distinct wings to the emission line profiles.

Presented axial emission profiles, for both *pd* values, show that with the increase of current, the intensity of emission also increases and reaches its maximum in an abnormal glow regime. Furthermore, the peak of emission in front of the anode [Figs. 4(I) (c) and 4(II) (c)] shifts toward the cathode with increasing current, which is a consequence of the formation and development of the cathode fall. Specifically, the position of the peak of the emission intensity in front of the anode corresponds to the maximum of negative glow, that matches with the edge of the cathode fall.[44] As the length of the cathode fall almost coincides with the distance between the electrodes at low pressures, these changes are not very pronounced [Figs. 4(I) (b) and 4(I) (c)].

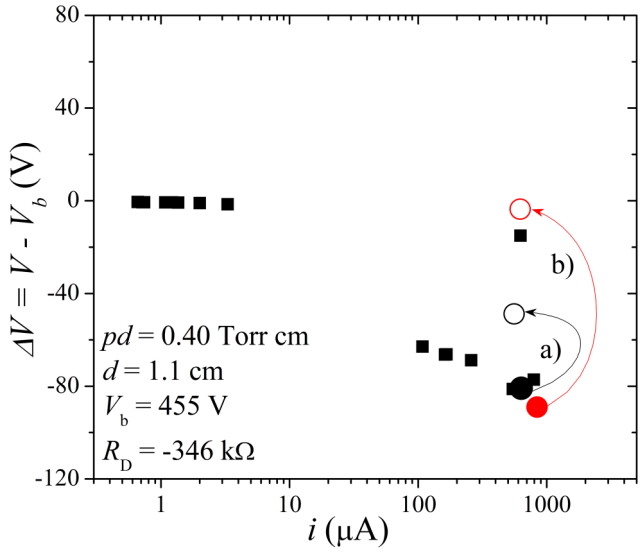

FIG. 5. Voltage–current characteristics for the methanol vapor discharge at *pd* = 0.40 Torr cm and *d* = 1.1 cm. Voltage Δ*V* represents the difference between the discharge voltage (*V*) and the breakdown voltage (V_b = 455 V). The discharge mode shift is denoted by arrows and symbols (circles) that correspond to values from Fig. 6.

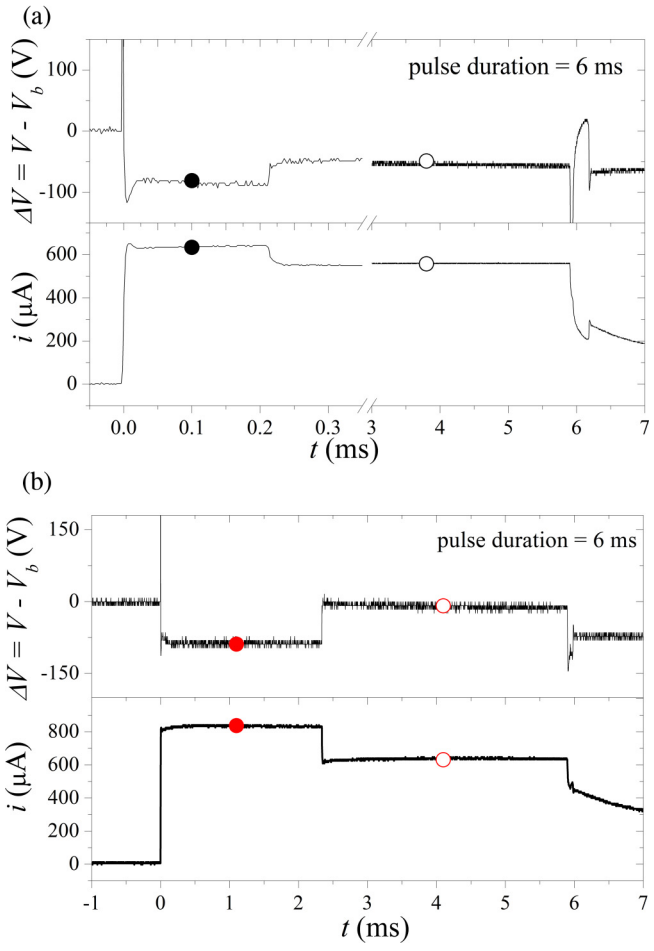

FIG. 6. Voltage and current waveforms obtained in the methanol vapor discharge at (a) lower initial current *i* = 630 μA and (b) higher initial current *i* = 840 μA with step-like transitions that occur during one pulse. Voltage Δ*V* represents the difference between the discharge voltage (*V*) and the breakdown voltage (V_b = 455 V). Voltage and current values before (full symbols) and after (open symbols) the step transition correspond to values from Fig. 5.

At higher pressure (0.40 Torr cm) after passing through the oscillation mode, the discharge enters the normal glow mode in a visibly constricted mode [Fig. 4(II) (b)]. In the constricted mode, the radial spatial distribution of the discharge is narrowed and occupies only a part of the surface on the electrode [Fig. 4(II) (b)]. The very appearance of the constricted discharge mode is conditioned by the existence of an extremely rapid increase in the ionization coefficient with the increase of the electric field.[36] The constriction is not very pronounced in the interval of high values of the reduced electric field E/N, i.e., lower $pd = 0.15$ Torr cm, due to a slight increase in the ionization coefficient at the transition from low-current diffuse to a normal glow discharge and longer diffusion length at lower pressure.

B. Mode transition

During our investigation of abnormal glow in methanol vapor, as part of the study of the voltage–current characteristics, we observed sudden changes in the operating conditions at $pd = 0.40$ Torr cm (Fig. 5). These changes in the operation mode were previously observed in an ethanol vapor discharge as shown in our previous article.[37] Measurements in methanol vapor at higher currents reveal changes in the steady-state current and voltage values within a single voltage pulse. The discharge operates at a lower current and a higher voltage after the transition.

We performed time-resolved measurements at higher currents in an abnormal regime to better perceive and understand what is happening in the discharge when this mode transition is occurring. The time-resolved measurements were done for points that are marked in Fig. 5 by open circles. At the same graph, full circles represent the voltage and current values before the discharge mode transition (before the step) that match the values marked at Fig. 6.

Figure 6 shows examples of step-like transitions in voltage and current waveforms that occur at two different initial currents: (a) 630 and (b) 840 μA. In the first case that is shown in Fig. 6(a), the mode transition is happening approximately 0.2 ms after the pulse ignition. During the transition, the discharge switches to ~30 V higher voltage and ~ 70 μA lower current. The transition is smooth and lasts around 4 μs. In the case of higher initial current [Fig. 6(b)], the transition occurs ~2 ms after the beginning of the pulse and after the transition (the "step") discharge operates at ~70 V higher voltage and ~200 μA lower current. The transition lasts approximately ~10 μs. It is important to emphasize that in both cases, the transition from one discharge mode to another is smooth without any observable instabilities or oscillations in voltage and current signals.

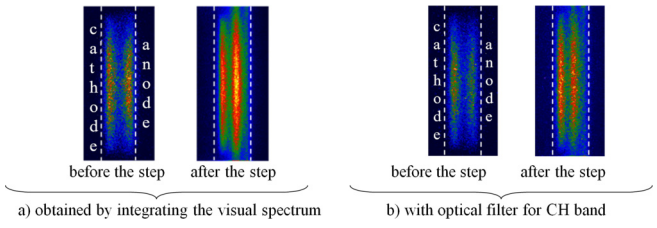

FIG. 7. 2D images of discharge, obtained along the chamber longitudinal axis, that corresponds to moments before and after the step-like transition [in Fig. 6(b)]: (a) images obtained by integrating the visual spectrum and (b) images obtained using an optical filter for the CH band at 431.2 nm.

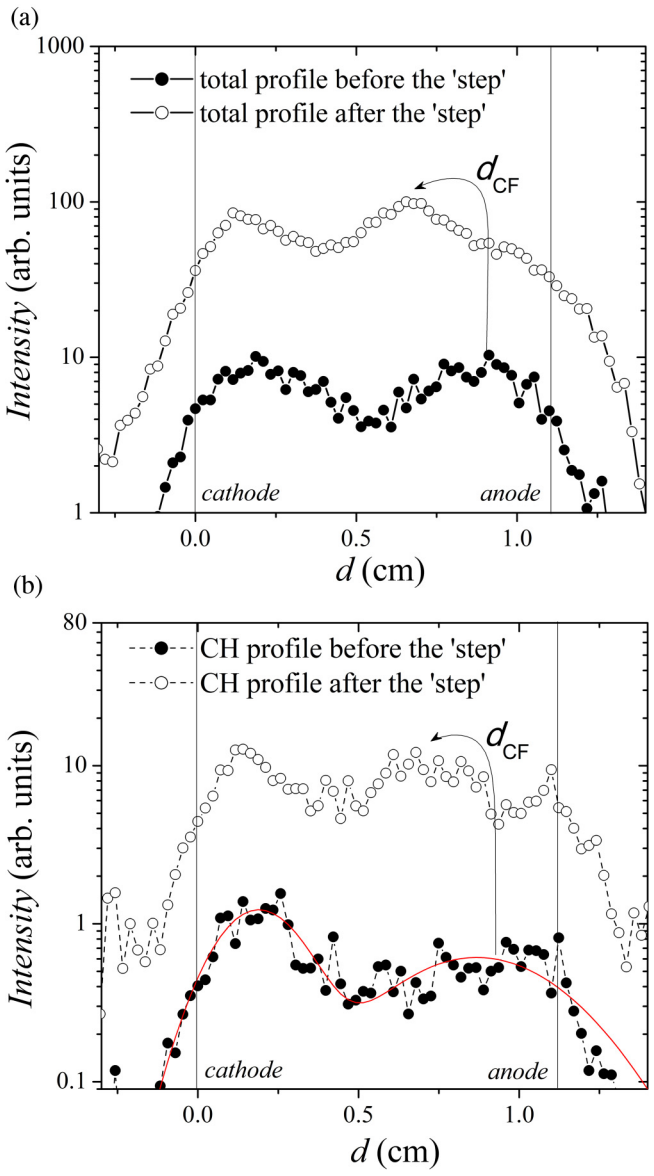

FIG. 8. Axial profiles of emission for methanol vapor obtained from 2D images (Fig. 7) at moments before (full symbols) and after (open symbols) the step-like transitions that correspond to the points given in Fig. 6(b). Here, we give a comparison of (a) the total emission profiles before (full symbols) and after (open symbols) and (b) the CH band emission profiles before (full symbols) and after (open symbols) the mode transition. The CH profile before the step is fitted with a function that is the sum of two Gaussians (red line) for easier identification of the maximum intensity in front of the anode. The changes in the initial values of voltage and current in the steady state after the step transition are $\delta V = 70$ V and $\delta i = -200$ μA. The length of cathode fall is denoted by d_{CF}.

Together with voltage and current measurements, we recorded 2D images of light emission from the discharge at several moments before and after the step-like transition within a single pulse (Fig. 7). These images provide axial profiles of emission of the discharge (Fig. 8) by extracting the intensity vector along the longitudinal axis of the discharge chamber. Thus, we may discern the changes in the mode of operation. We also used an optical filter for the CH band at 431.2 nm that enabled comparison with total axial profiles of emission obtained by integrating the whole visual spectrum [2D images in Fig. 7(a)].

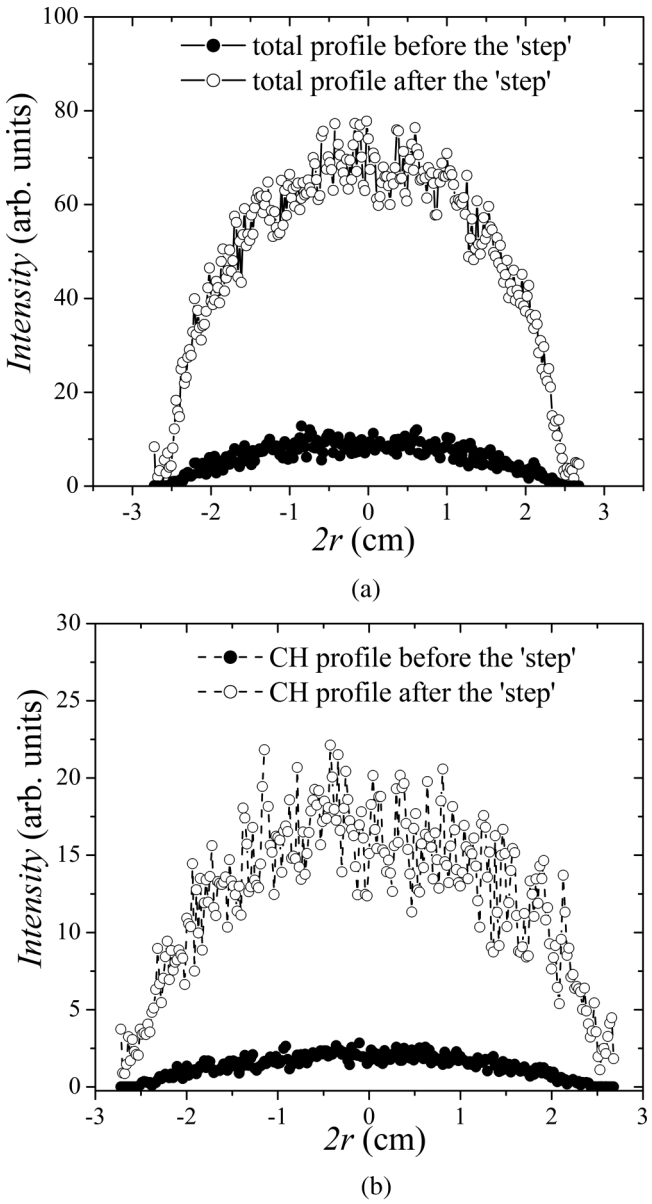

FIG. 9. Radial profiles of emission in the methanol vapor discharge: (a) total radial profiles and (b) CH radial profiles, in moments before (full symbols) and after (open symbols) the step-like transition that corresponds to points given at Fig. 6(b).

Figure 8 shows (a) total and (b) CH axial profiles of emission before and after the "step" transition. In both cases, profiles before and after the "step" have a peak close to the cathode, indicating that excitation by heavy particles[26,50] is significant. Also, after the transition, the overall intensity of emission is higher, even though the discharge current drops. The ratio of the contribution of heavy particles and electrons to the emission intensity remains the same.

Moreover, from the radial profiles of emission (Fig. 9) obtained from the 2D images of the discharge taken before and after the "step" transition (Fig. 7), it can be seen that both profiles have the same width and, therefore, the same effective discharge area.[33] This means that the normal glow has reached its maximum width and is about to make transition to the abnormal glow.

The main difference in the profiles before and after the step is the position of the emission peak that corresponds to the negative glow, i.e., coincides with the edge of the cathode fall d_{CF}.[44] The edge of the cathode fall region shifts closer to the cathode after the transition, which seems to be in contradiction to the decrease of discharge current but is consistent with an increase in *E/N*. In any case, we may conclude that the transition shown here represents a direct observation of the transition from a normal to an abnormal glow discharge mode. The fact that the current decreases in transition to the abnormal glow means that the space charge is formed, and with a sufficient increase in the local *E/N* (higher voltage and shorter cathode fall), it compensates for the losses in excitation and ionization due to somewhat decreased current. It is not linear extrapolation as here, we deal with sheaths of different voltage and length values.

IV. CONCLUSION

In this paper, we have provided experimental recordings of the voltage–current (*V–i*) characteristics of discharges in four different, yet common, alcohols covering Townsends, normal glow, and abnormal glow regimes (low current diffuse, constricted, and high-current diffuse in Phelps' terminology). Such data for alcohols have not been hitherto available.

The Townsend regime characteristics apart from values of breakdown voltage provide the negative differential resistance as a quantitative measure of the space charge effects.[51] We may notice a strong dependence of R_D with *pd*. Spatial emission profiles in this regime may also be fitted by theoretical/numerical results and used to obtain data on elementary atomic and molecular collision processes such as ionization rates and cross sections and total excitation/dissociation rates induced both by electrons and by heavy particles, in particular, fast neutrals.[50] All these data are lacking for the alcohols (both as vapors and liquids as the background for discharges, leading to the production of a non-equilibrium plasma). Present results for spatial emission profiles, if normalized to absolute values, may be the basis to produce quantitative data. Such normalization is possible as we maintained relative calibration of the sensitivity. Here, we present results for the overall emission (that, as expected, has the best statistics) and for the CH band emission that is the strongest component of the total emission.

Both show significant heavy particle excitation increasing with the *E/N*. Nevertheless, we have found an emission band that is not excited by the heavy particles in the region of mean energies and operating fields covered here.

Following the progression of the *V–i* characteristics to the region of the normal glow (through the unstable domain of the Townsend to normal glow transition), one can see the correspondence between the spatial profiles of the discharges in different modes and the *V–i* characteristics. The difference in the voltage between the normal glow and the breakdown voltage is an important factor as well as the slope of the load line for the stability of operation of the discharge.

Finally, we have observed a distinct transition between a normal and an abnormal glow regime occurring within a limited time and leading to observable rearrangement of the field and plasma profile, also leading to much more efficient production of photons (and presumably ionization). The mode transition so far has been observed for argon[56] and for ethanol too.[37] In this case, we have provided the most systematic measurement as a basis for possible modeling of those data. It may also be used to test and verify plasma modeling codes in the domain of representing space charge effects.[57,58] The "step" in the voltage indicates the transition between two regimes of operation that may not be in stable equilibrium to begin with. The transition is clearly between the normal and abnormal glow regimes and may be induced by a number of processes (heating of the gas, conditioning of the cathode, external perturbation, gradual slow growth of the space charge, etc.). It may also be associated with different radial profiles of the discharge. Such transitions are more easily observed when the discharge oscillates with different regimes of oscillations in the pre- and post-transition domains. This is not the case here. Interestingly, in the present case, for both methanol and ethanol, radial profiles in the two regimes are not observably different. In any case, gases where such transitions were observed, for a very narrow range of conditions, are very few.

The elementary processes in alcohol vapors and liquids may lead to a wealth of products and may initiate further chemical reaction chains that may be used for a number of purposes. Of the more direct applications, one may benefit from the extended knowledge of the breakdown in alcohol vapors having in mind applications such as using alcohols as combustion fuels, nanostructure growth in discharges through liquids, and in using admixtures of different molecules in atmospheric pressure plasmas for various biotechnical procedures. On a separate plane, one should mention the development of the elementary particle detectors, the new generations where optimized design may improve performance significantly.

ACKNOWLEDGMENTS

The authors acknowledge support from the Serbian Ministry of Education, Science and Technological Development under Project Nos. OI 171037 and III 41011. Z.Lj.P. is grateful to the SASA project 155 and to the Ulster University for partial support.

DATA AVAILABILITY

The data that support the findings of this study are available from the corresponding author upon reasonable request.

REFERENCES

[1]P. J. Bruggeman, M. Kushner, B. Locke, H. Gardeniers, B. Graham, D. Graves, R. Hofman-Caris, D. Marić, J. Reid, E. Ceriani, D. Fernandez Rivas, J. Foster, S. Garrick, Y. Gorbanev, S. Hamaguchi, F. Iza, H. Jablonowski, E. Klimova, F. Krcma, J. Kolb, P. Lukes, Z. Machala, I. Marinov, D. Mariotti, S. Mededovic Thagard, D. Minakata, E. Neyts, J. Pawlat, Z. L. Petrović, R. Pflieger, S. Reuter, D. Schram, S. Schroeter, M. Shiraiwa, B. Tarabova, P. Tsai, J. Verlet, T. von Woedtke, K. Wilson, K. Yasui, and G. Zvereva, Plasma Sources Sci. Technol. **25**, 053002 (2016).
[2]G. Petitpas, J. D. Rollier, A. Darmonb, J. Gonzalez-Aguilar, R. Metkemeijer, and L. Fulcheri, Int. J. Hydrog. Energy **32**, 2848 (2007).
[3]S. Maruyama, R. Kojimaa, Y. Miyauchia, S. Chiashia, and M. Kohnob, Chem. Phys. Lett. **360**, 229 (2002).
[4]M. Matsushima, M. Noda, T. Yoshida, H. Kato, G. Kalita, T. Kizuki, H. Uchida, M. Umeno, and K. Wakita, J. Appl. Phys. **113**, 114304 (2013).
[5]A. Ando, K. Ishikawa, H. Kondo, T. Tsutsumi, K. Takeda, T. Ohta, M. Ito, M. Hiramatsu, M. Sekine, and M. Hori, Jpn. J. Appl. Phys. **57**, 026201 (2018).
[6]A. Kumar, P. A. Lin, A. Xue, B. Hao, Y. K. Yap, and R. M. Sankaran, Nat. Commun. **4**, 2618 (2013).
[7]N. Tarasenka, A. Stupak, N. Tarasenko, S. Chakrabarti, and D. Mariotti, Chem. Phys. Chem. **18**, 1074 (2017).
[8]M. G. Sobacchi, A. V. Saveliev, A. A. Fridman, L. A. Kennedy, S. Ahmed, and T. Krause, Int. J. Hydrog. Energy **27**, 635 (2002).
[9]F. Chen, X. Huang, D. Cheng, and X. Zhan, Int. J. Hydrog. Energy **39**, 9036 (2014).
[10]R. Dillon, S. Srinivasan, A. S. Aricò, and V. Antonucci, J. Power Sources **127**, 112 (2004).
[11]M. Z. F. Kamarudin, S. K. Kamarudin, M. S. Masdar, and W. R. W. Daud, Int. J. Hydrog. Energy **38**, 9438 (2013).
[12]R.-C. Zhang, D. Sun, R. Zhang, W.-F. Lin, M. Macias-Montero, J. Patel, S. Askari, C. McDonald, D. Mariotti, and P. Maguire, Sci. Rep. **7**, 46682 (2017).
[13]D. J. Grey, R. K. Sood, and R. K. Manchanda, Nucl. Instrum. Methods Phys. Res. A **527**, 493 (2004).
[14]D. Bošnjaković, Z. L. Petrović, R. D. White, and S. Dujko, J. Phys. D: Appl. Phys. **47**, 435203 (2014).
[15]J. Va'vra, Nucl. Instrum. Methods Phys. Res. A **515**, 1 (2003).
[16]M. G. Curtis and I. C. Walker, J. Chem. Soc. Faraday Trans. **88**, 2805 (1992).
[17]T. L. Cottrell and I. C. Walker, Trans. Faraday Soc. **61**, 1585 (1965).
[18]J. Sivoš, D. Marić, G. Malović, and Z. L. Petrović, Eur. Phys. J. D **74**, 64 (2020).
[19]I. Adamovich, S. D. Baalrud, A. Bogaerts, P. J. Bruggeman, M. Cappelli, V. Colombo, U. Czarnetzki, U. Ebert, J. G. Eden, P. Favia, D. B. Graves, S. Hamaguchi, G. Hieftje, M. Hori, I. D. Kaganovich, U. Kortshagen, M. J. Kushner, N. J. Mason, S. Mazouffre, S. Mededovic Thagard, H.-R. Metelmann, A. Mizuno, E. Moreau, A. B. Murphy, B. A. Niemira, G. S. Oehrlein, Z. L. Petrovic, L. C. Pitchford, Y.-K. Pu, S. Rauf, O. Sakai, S. Samukawa, S. Starikovskaia, J. Tennyson, K. Terashima, M. M. Turner, M. C. M. van de Sanden, and A. Vardelle, J. Phys. D: Appl. Phys. **50**, 323001 (2017).
[20]J. Tennyson, S. Rahimi, C. Hill, L. Tse, A. Vibhakar, D. Akello-Egwel1, D. B. Brown, A. Dzarasova, J. R. Hamilton, D. Jaksch, S. Mohr, K. Wren-Little, J. Bruckmeier, A. Agarwal, K. Bartschat, A. Bogaerts, J. P. Booth, M. J. Goeckner, K. Hassouni, Y. Itikawa, B. J. Braams, E. Krishnakumar, A. Laricchiuta, N. J. Mason, S. Pandey, Z. L. Petrovic, Y.-K. Pu, A. Ranjan, S. Rauf, J. Schulze, M. M. Turner, P. Ventzek, J. C. Whitehead, and J.-S. Yoon, Plasma Sources Sci. Technol. **26**, 055014 (2017).

[21]S. Ghosh, K. L. Nixon, W. A. D. Pires, R. A. A. Amorim, R. F. C. Neves, H. V. Duque, D. G. M. da Silva, D. B. Jones, F. Blanco, G. Garcia, M. J. Brunger, and M. C. A. Lopes, Int. J. Mass Spectrom. **430**, 44 (2018).
[22]X.-D. Wang, C.-J. Xuan, W.-L. Feng, and S. X. Tian, J. Chem. Phys. **142**, 064316 (2015).
[23]D. G. M. da Silva, M. Gomes, S. Ghosh, I. F. L. Silva, W. A. D. Pires, D. B. Jones, F. Blanco, G. Garcia, S. J. Buckman, M. J. Brunger, and M. C. A. Lopes, J. Chem. Phys. **147**, 194307 (2017).
[24]M. J. Brunger, Int. Rev. Phys. Chem. **36**, 333 (2017).
[25]J. Sivoš, N. Škoro, D. Marić, G. Malović, and Z. L. Petrović, J. Phys. D: Appl. Phys. **48**, 424011 (2015).
[26]D. Marić, P. Hartmann, G. Malović, Z. Donkó, and Z. L. Petrović, J. Phys. D: Appl. Phys. **36**, 2639 (2003).
[27]D. Marić, M. Savić, J. Sivoš, N. Škoro, M. Radmilović-Radjenović, G. Malović, and Z. L. Petrović, Eur. Phys. J. D **68**, 155 (2014).
[28]A. V. Phelps and Z. L. Petrović, Plasma Sources Sci. Technol. **8**, R21 (1999).
[29]M. M. Nikolić, A. R. Đorđević, I. Stefanović, S. Vrhovac, and Z. L. Petrovic, IEEE Trans. Plasma Sci. **31**, 717 (2003).
[30]A. V. Phelps, L. C. Pitchford, C. Pedoussat, and Z. Donko, Plasma Sources Sci. Technol. **8**, B1 (1999).
[31]A. V. Phelps, Z. L. Petrović, and B. M. Jelenković, Phys. Rev. E **47**, 2825 (1993).
[32]M. S. Mokrov and Y. P. Raizer, Plasma Sources Sci. Technol. **17**, 035031 (2008).
[33]N. Škoro, D. Marić, and Z. L. Petrović, IEEE Trans. Plasma Sci. **36**, 994 (2008).
[34]P. Hartmann, Z. Donkó, G. Bánó, L. Szalai, and K. Rózsa, Plasma Sources Sci. Technol. **9**, 183 (2000).
[35]Z. L. Petrović, I. Stefanović, S. Vrhovac, and J. Živković, J. Phys. IV France **7**, C4–341 (1997).
[36]D. Marić, G. Malović, and Z. L. Petrović, Plasma Sources Sci. Technol. **18**, 034009 (2009).
[37]J. Sivoš, D. Marić, N. Škoro, G. Malović, and Z. L. Petrović, Plasma Sources Sci. Technol. **28**, 055011 (2019).
[38]H. Hasegawa and H. Date, J. Appl. Phys. **117**, 133302 (2015).
[39]R. Rejoub, C. D. Morton, B. G. Lindsay, and R. F. Stebbings, J. Chem. Phys. **118**, 1756 (2003).
[40]C. Ni, D. Carolan, C. Rocks, J. Hui, Z. Fang, D. B. Padmanaban, J. Ni, D. Xie, P. Maguire, J. T. S. Irvine, and D. Mariotti, Green Chem. **20**, 2101 (2018).
[41]A. A. General, A. K. Shuaibov, V. A. Kel'man, and Y. V. Zhmenyak, Tech. Phys. Lett. **40**, 482 (2014).
[42]A. I. Shchedrin, D. S. Levko, V. Y. Chernyak, V. V. Yukhimenko, and V. V. Naumov, Tech. Phys. Lett. **35**, 449 (2009).
[43]J. R. Ferrell, E. R. Bogovich, N. R. Lee, R. L. Gray, and D. D. Pappas, Biointerphases **10**, 021001 (2015).
[44]D. Marić, K. Kutasi, G. Malović, Z. Donkó, and Z. L. Petrović, Eur. Phys. J. D **21**, 73 (2002).
[45]S. Živanov, J. Živković, I. Stefanović, S. Vrhovac, and Z. L. Petrović, Eur. Phys. J. Appl. Phys. **11**, 59 (2000).
[46]I. Stefanović and Z. L. Petrović, Jpn. J. Appl. Phys. **36**, 4728 (1997).
[47]R. C. Weast, *Handbook of Chemistry and Physics*, 51st ed. (Ohio Chemical Rubber Co., Cleveland, OH, 1970).
[48]Z. L. Petrović and A. V. Phelps, Phys. Rev. E **47**, 2806 (1993).
[49]B. M. Jelenković, K. Rózsa, and A. V. Phelps, Phys. Rev. E **47**, 2816 (1993).
[50]Z. L. Petrović and A. V. Phelps, Phys. Rev. E **80**, 016408 (2009).
[51]Z. L. Petrović, B. M. Jelenković, and A. V. Phelps, Phys. Rev. Lett. **68**, 325 (1992).
[52]A. V. Phelps and B. M. Jelenković, Phys. Rev. A **38**, 2975 (1988).
[53]Z. L. Petrović and A. V. Phelps, Phys. Rev. E **80**, 066401 (2009).
[54]V. Stojanović, Ž Nikitović, and Z. L. Petrović, IEEE Trans. Plasma Sci. **39**, 2592 (2011).
[55]Z. L. Petrović and V. D. Stojanović, J. Vac. Sci. Technol. A **16**, 329 (1998).
[56]Z. L. Petrović and A. V. Phelps, Phys. Rev. E **56**, 5920 (1997).
[57]A. Fierro, E. Barnat, M. Hopkins, C. Moore, G. Radtke, and B. Yee, "Challenges and opportunities in verification and validation of low temperature plasma simulations and experiments," Eur. J. Phys. D (to be published).
[58]M. Turner, Plasma Sources Sci. Technol. **25**, 054007 (2016).

Eur. Phys. J. D (2021)75:191
https://doi.org/10.1140/epjd/s10053-021-00138-z

THE EUROPEAN PHYSICAL JOURNAL D

Regular Article - Plasma Physics

Effective ionization coefficients for low current dc discharges in alcohol vapours at low pressure

Jelena Marjanović[1], Dragana Marić[1], Gordana Malović[1], and Zoran Lj. Petrović[2,3,a]

[1] Institute of Physics, University of Belgrade, Pregrevica 118, 11080 Belgrade, Serbia
[2] School of Engineering, Ulster University, Jordanstown, Co. Antrim BT37 0QB, UK
[3] Serbian Academy for Sciences and Arts, Knez Mihailova 35, 11001 Belgrade, Serbia

Received 31 January 2021 / Accepted 26 March 2021

Abstract. This paper presents results for effective ionisation coefficients ($\alpha_{\rm eff}/N$, N—gas density) obtained from the breakdown voltage and emission profile measurements in low-pressure dc discharges in vapours of alcohols: methanol, ethanol, isopropanol, and n-butanol. Our results for $\alpha_{\rm eff}/N$ are determined from the axial emission profiles in low-current Townsend discharge and lay in the interval of reduced electric field E/N (E—electric field, N—gas density), from 1 kTd to 8.8 kTd. We also give a comparison of our experimental results with those from the available literature. Our data cover the high E/N range of the standard operating conditions and in the region where other data are available we have a good agreement.

1 Introduction

Discharges in liquids and their vapours, primarily in water and alcohols, have opened a wide field of new applications for energy sources and fuel industry [1,2], for polymerization and thin-film synthesis [3], for the synthesis of nanographene layers and fast growth of carbon nanotubes [4–6], for the treatment of materials and surfaces [7,8], biomedicine [7,9], applications in agriculture [10,11] etc. All those applications and devices operate either in liquid, liquid-bubbles systems or with a significant gas/vapor interface, under different discharge conditions [12]. Those open new questions connected to elementary processes, dominant particles atomic and molecular collisions, surface interactions, and breakdown conditions. The elementary electron molecule collisions are often determined from fitting of the calculated swarm parameters to the experimental data. Usually, at low mean energies drift velocity and transverse diffusion normalized to electron mobility are used to determine total momentum transfer and some version of the total cross sections for inelastic processes [13–16]. Use of pulsed Townsend (PT) experiments [17,18] facilitated the use of drift velocities and ionization coefficients to obtain/normalize the cross section data at moderate and higher E/N. In particular, our group promoted fitting [19] the moderate energy range of the cross sections 5–30 eV by adjusting the dissociative excitation while keeping the ionization cross sections as they are produced in binary collision experiments [20–24] or theory (e.g., Binary Encounter Bethe—BEB) [25]. It is important to note that the region where ionization becomes relevant in ionized gas kinetics is the operating region of most plasmas, ionization is needed to compensate the losses and maintain self-sustained discharges. On the other hand, under those conditions non-conservative effects on the transport coefficients become apparent [26,27] making the whole procedure more difficult. In any case ionization coefficients in this region of E/N are required to set the inelastic losses of the electron ensemble and to set its mean energy.

It is known that breakdown, under dc fields and slowly varying ac fields, depends on surface collisions of ions and atoms, so the breakdown condition is a very sensitive projection of the atomic and molecular collisions [28–31]. Our research aims at providing some of the elementary data on dc breakdown and low-pressure operation regimes in a wide interval of discharge currents in alcohol vapours, for such data are scarce in the literature. In our measurements of breakdown and low-current regimes of dc discharges, we can determine coefficients for elementary processes of universal importance in all regimes of operation, such as ionization rate, secondary electron yield, excitation rates by fast neutrals, and eventually the corresponding cross sections.

In our earlier papers [32,33] we have presented measurements of breakdown voltages and spatial profiles of low-current dc discharges in alcohol vapours: methanol, ethanol, isopropanol, and n-butanol as well as in water vapour. In our previous papers on alcohols, spatial emission profiles have been used to illustrate the transition between different discharge modes. In this paper we start from the axial profiles for the low current diffuse (Steady State Townsend—SST) regime recorded, as described in [32,33] and produce effective ionization coefficients.

[a] e-mail: z.petrovic@ulster.ac.uk (corresponding author)

Published online: 29 June 2021

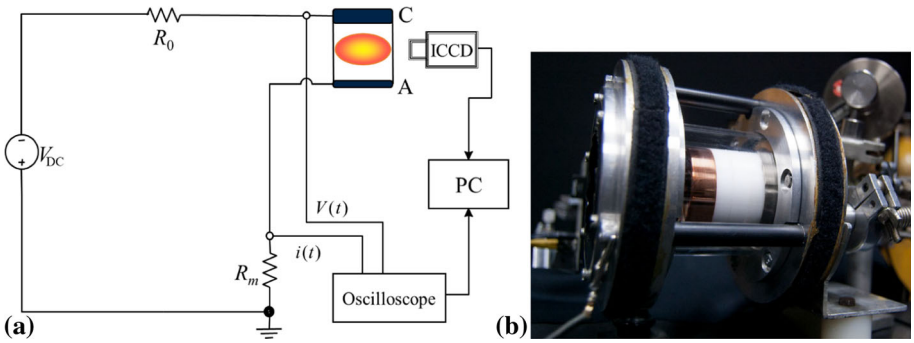

Fig. 1 **a** Schematics of the experimental setup and the electrical circuit used in measurements. All the recordings were made with an ICCD camera mounted with an objective lens. The series resistor R_0 is used to limit the current [37] while R_m is the "monitoring" resistor used to measure the discharge current; **b** photograph of the discharge chamber

2 Experimental set-up

Experimental measurements are done in a parallel-plate electrode system that is placed inside a tightly fitted quartz tube [34]. The diameter of electrodes D is 5.4 cm, the cathode (C) is made of copper, while the anode (A) is made of quartz with a transparent, conductive platinum thin film deposited on its surface. The distance between electrodes is adjustable and the present measurements were performed with $d = 1.1$ cm and 3.1 cm. Figure 1a shows a simplified schematic of our set-up [33,34].

Construction of the discharge chamber (Fig. 1b) allows side-on measurements of emission intensity, along the longitudinal chamber axis. For recordings of light emission, we used a sensitive ICCD camera (Andor IStar DH720-18U-03) equipped with a glass lens that allows us to acquire axial discharge profiles of spectrally integrated emission in the visible range of spectrum, defined by the transparency of the lens and the quantum efficiency of the ICCD photocathode. Adding the optical filters allows us to measure profiles associated with some specific lines [32,33]. Further recordings with optical filters (Hα, CH at 431.2 nm) were done to provide us with additional information on particular processes of excitation [32,33] and even the possibility to obtain absolute spatial profiles of excitation coefficients [35]. Profiles of Hα emission proved to be valuable as they show only a small contribution of fast neutrals to excitation [33], which enabled us to extend the range of measurement of effective ionization coefficients to somewhat higher E/N. Still, in all cases, we obtained the same ionization coefficients regardless of whether filters were used or not. We mostly used measurements of emission integrated in the visible range of the spectrum, as the statistics was the best in that case, while filters were used mainly as an internal consistency check in this paper.

Prior to the measurements, the discharge chamber is evacuated to the base pressure of $\sim 10^{-6}$ Torr, and then the cathode surface is treated by a relatively high current discharge (30 μA) in low pressure (around 1 Torr) hydrogen, approximately for 30 min, until a stable operating voltage is reached. The treatment of the cathode surface is likely to remove oxide layers, although stable oxide layers such as those found on stainless steel, aluminium and copper are impossible to remove altogether but may be made more uniform Beside oxide removal, such a treatment also removes organic molecules originating from the pumping oils and other impurities from the cathode resulting in a stable surface during long periods of measurements in one day. The procedure can provide reliable and reproducible breakdown data [30,31]. Both, treatment in hydrogen discharge and measurements in alcohol vapours are done in a slow flow regime, to ensure that possible impurities formed in the discharge chamber are continuously removed.

Measurements were done for four selected alcohols: methanol, ethanol, isopropanol (2-propanol) and n-butanol. The vapours were obtained from 99.5% purity methanol, isopropanol, n-butanol, and 95% purity ethanol. All used alcohols are pro analysi grade chemicals and for all of them water represents the most abundant declared impurity (max. 0.2%), while other volatile impurities such as acetone, aldehydes, and formic acid (max. 0.002%) are present in smaller quantities. The amount of gaseous impurities dissolved in the liquid were reduced by repeated pumping of the gas above the liquid sample. Although, present only in traces, there is iron (0.0005%) and some non-volatile substances (< 0.001%) as well. However, the presence of a small amount of water vapour and of other impurities in the discharge does not affect the results [33]. The vapour is obtained from the liquid alcohol sample placed in a test tube. After opening a regulatory pressure valve, alcohol begins to boil due to the pressure difference above its surface (10^{-6} Torr) and the pressure of dissolved gases in the sample itself. In this way, alcohol becomes devoid of dissolved volatile constituents. The impurities are thus reduced in the liquid sample to a minimum through the boiling and evacuating sequences. When boiling ends, vapour is maintained at a moderate pressure (lower than the vapour pressure) in the chamber for 1–2 h to saturate the electrodes and the chamber walls. The vapour pressures for methanol, ethanol, isopropanol, and n-butanol at room temperature are around 127, 45, 44 and 7 Torr, respectively

[36]. The temperature in the laboratory is maintained by the air-conditioning system at the temperature of 20 degrees Celsius. In all cases we operate at pressures well below the vapour pressure (that may drastically change with variation of the temperature), so our pressure and results are not dependent on small variations of the room temperature. A more detailed description of the experimental procedure is given in [32,33].

Electric circuit is designed (see our previous papers [32,34,38]) to provide stable operation of the discharge near the breakdown conditions [31–33,39]. The series resistor R_0 with a high resistance is used to limit current keeping it as low as possible for measurements in the Townsend discharge. The resistor R_m is used to measure the discharge current. This resistor strongly affects the oscillations of the current [28,37]. For detection of the electrical signal, we used a digital oscilloscope (Keysight Technologies DSO9104A) and two voltage probes (Tektronix P6915 and Agilent 10076A).

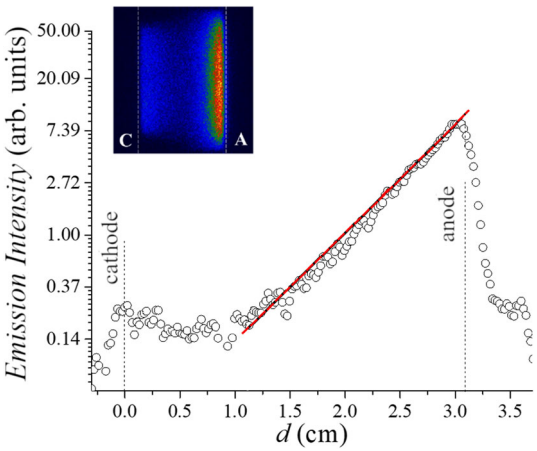

Fig. 2 2D image and axial emission profile of low-current Townsend discharge recorded in methanol vapor for $pd = 0.70$ Torr cm, $V_b = 460$ V and $E/N = 2$ kTd at electrode distance of $d = 3.1$ cm. The plot of the emission profile in the semi-log scale reflects electron multiplication between the electrodes, and the profile slope (red line) corresponds to the effective ionization coefficient

3 Results and discussion

In addition to the prebreakdown measurements [40] one can also use low-current self-sustained discharges operating in the low-current limit (no space charge, constant electric field i.e., a Steady State Townsend SST swarm experiment) to obtain the ionization coefficients. Initial stages of breakdown go through the multiplication of electrons dictated by the external field, and for the low-current limit of the discharges in the dark Townsend or the low-current diffuse regime the growing space charge may be used as a perturbation to the external field distribution [28,30,41,42]. Recording of the Volt-Ampere characteristics and of the spatial profiles allow us to find the conditions where space charge effects are negligible.

Based on experimentally recorded emission profiles for the low-current limit (no space charge) of the DC discharges in the Townsend/diffuse regime (breakdown conditions) [32,33], we were able to determine effective ionization coefficients. Figure 2 shows an example of an experimentally recorded emission profile in low-current Townsend discharge in methanol vapour. Exponential growth is best observed if plotted in a semi-logarithmic scale and the slope corresponds to the effective ionization coefficient α_{eff}/N (Fig. 2), once equilibrium with the local field is reached [31,35,43]. The use of emission profiles recorded at high values of reduced electron fields to determine the α_{eff}/N is limited due to emission in front of the cathode, coming from heavy-particle excitation, that masks the part of profile connected to electron-induced ionization and excitation [44,45]. Another limitation at the highest E/N is due to extended equilibration distance (the flat region up to 1 cm in Fig. 2 that may take up a large part of the gap.

As ionization coefficient is the gas phase electron collision coefficient it should be independent of the preparation of the surfaces and the material used. This was confirmed throughout our measurements. Since the electrode material (cathode in particular) does influence the operating point and the stability of the discharge, electrode treatment was done before each set of measurements. Finally, due to absorption by the electrodes one may have an increase of the mean electron energy towards the absorbing anode that may or may not affect the ionization/excitation coefficients in the region. At the very high E/N one may have reflection and secondary electron production after electron impact on the anode, resulting in a small structure adjacent to the anode. Measurements of ionization coefficients should stay clear or be able to eliminate all these possible sources of deviations from the exponential growth profiles. We made sure that none of these problems affected our measurements. Uncertainties that enter the determination of the effective ionization coefficients are only statistical and thus may be observed in the graphs. The uncertainty of E/N is determined by the gap, voltage and pressure measurements and is of the order of 3%.

Figure 3 shows dependence of the effective ionization coefficients α_{eff}/N on reduced electric field E/N for the discharges in methanol, ethanol, isopropanol, and n-butanol vapours, obtained in the range of E/N from 1 kTd to 8.8 kTd. For comparison we also show results for effective ionization coefficients from the literature that are available only for methanol and ethanol [46,47] and [48] as compiled in [49]. Additionally, we give numerical data listed in Table 1 that correspond to the results shown in Fig. 3.

Hasegawa's and Date's results for methanol [46] cover the region of much lower values of the reduced electric fields, from 130 Td to 3 kTd. For the overlapping range of E/N, our effective ionization coefficients in methanol vapor are slightly lower than those in the work of Hasegawa and Date (Fig. 3a). The difference

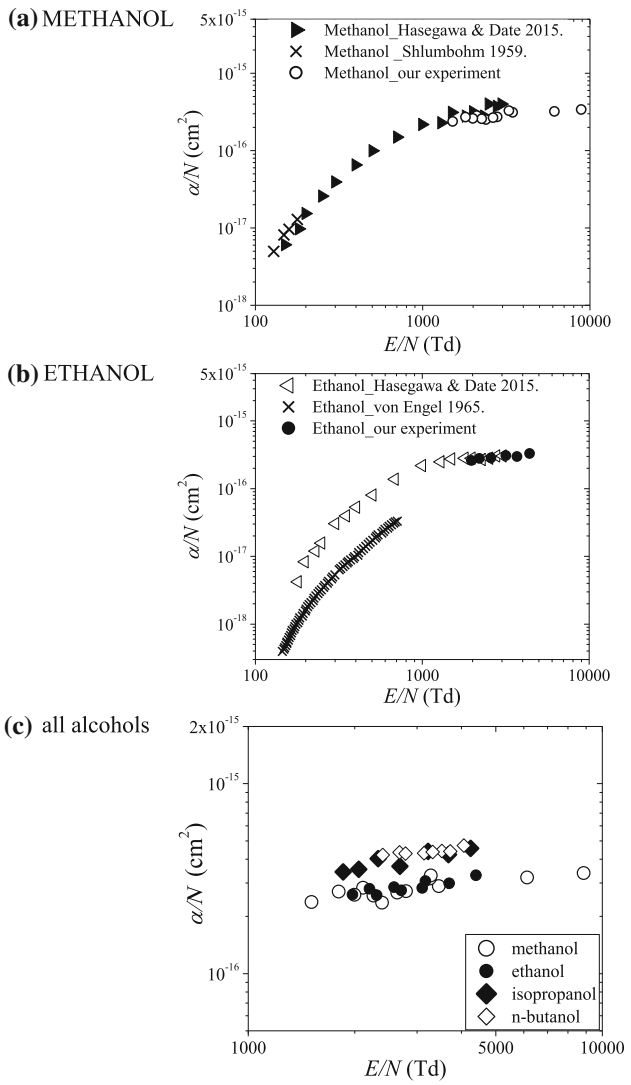

Fig. 3 The dependence of reduced effective ionization coefficient (α_{eff}/N) on the reduced electric field (E/N). Results obtained from our experiment for a) methanol (open black circles) and b) ethanol (solid black circles) are compared with data for methanol from Hasegawa and Date [46] (solid black triangles) and Shlumbohm [47] (black X) and with data for ethanol from Hasegawa and Date [46] (open black triangles) and von Engel [49] (black X). Additionally, c) shows the results obtained from our experiment for isopropanol and n-butanol presented together with the results for methanol and ethanol

increases to almost a factor of two above 2 kTd. The results of Shlumbohm [47] for methanol (Fig. 3a) are slightly higher than those of Hasegawa and Date for the range of $E/N < 200$ Td, while we do not have results at such low reduced electric fields values.

In case of ethanol vapour, our results agree well with those of Hasegawa's and Date's for the E/N range of 1.5–3 kTd. Furthermore, results from Hasegawa [46] and Raether [48] (as presented by von Engel in [49]), in the overlapping range of E/N (140–700 Td), differ from each other (Fig. 3b) by a large factor, even greater than 3, the effective ionization coefficients from Raether [48] being much smaller. This disagreement may be due to differences in experiments and measurement techniques or the purity of the ethanol samples, especially having in mind that the data from Raether date from 1930s and were obtained by recording light emission from the avalanches without control of the space charge effects (that are in our case provided by the Volt- Ampere characteristics for a steady discharge).

In Fig. 3c, we present results for α_{eff}/N for electrons in isopropanol and n-butanol vapours. The results for effective ionization coefficients for these higher-order alcohols cover a relatively narrow and yet important range of reduced electric fields, from 1.8 to 4.3 kTd. Figure 3c also shows results for all alcohols studied in this work. In the entire E/N range, effective ionization coefficients for isopropanol and n-butanol are a little higher than for the methanol and ethanol.

4 Conclusion

Non-equilibrium discharges and plasmas that operate in liquid media or an environment that contains vapours have become a significant subject of research due to the broad field of possible applications [4,12,50]. Obtaining new and improvement of existing applications require accessible data for modeling, good understanding, and an insight into elementary processes. Accordingly, in this paper, we present the results for effective ionization coefficients obtained from our experimental study of low-pressure dc breakdown in vapours of alcohols—in three primary alcohols: methanol, ethanol, n-butanol, and one secondary alcohol: isopropanol. Effective ionization coefficient is obtained from axial emission profiles in low-current Townsend discharges for conditions with dominant electron excitation of the background gas (high pressure i.e., lower E/N). Our results lay in the reduced electric field interval 1–8.8 kTd.

In the available literature, there is not much data on ionization coefficients for discharges in alcohol vapours. Based on our knowledge, the effective ionization coefficients for higher-order alcohols (isopropanol, and n-butanol), are given for the first time in this paper. For isopropanol and n-butanol, we obtained results that cover a relatively narrow range of moderate values of E/N from 1.8 to 4.3 kTd.

On the other hand, for methanol and ethanol we were able to compare our results with the results from the literature. Although the E/N ranges covered in our experiment and experimental measurements of Hasegawa and Date [46] in the most part do not overlap, for the interval where they do, agreement of results from both sources is reasonably good. However, we could not obtain results for α_{eff}/N that correspond to lower values of E/N ($E/N < 1$ kTd), due to limitations of the experiment and the electrical circuit components that did not allow us to have a stable dc dark Townsend discharge (i.e., without oscillations) [39]. On the other hand, our measurements have enabled extending the

Table 1 Effective ionization coefficients obtained in our experimental measurements of discharges in vapours of alcohols: methanol, ethanol, isopropanol, and n-butanol. During the measurements, the room temperature was $T = 20\,^{\circ}\mathrm{C}$

	p(Torr)	V_b (V)	E/N(Td)	α (pairs/cm)	$\alpha_{\mathrm{eff}}/N \times 10^{-16}$(cm^2)	d(cm)
Methanol	0.18	585	8866	2.03	3.38	1.1
	0.22	505	6136	2.4	3.21	1.1
	0.36	455	3453	3.46	2.89	1.1
	0.45	460	2792	4.07	2.72	1.1
	0.54	472	2389	4.25	2.36	1.1
	0.63	488	2110	5.94	2.83	1.1
	0.13	433	3278	1.4	3.28	3.1
	0.16	435	2636	1.42	2.67	3.1
	0.19	446	2257	1.64	2.57	3.1
	0.22	460	1996	1.93	2.59	3.1
	0.26	475	1802	2.3	2.7	3.1
	0.32	497	1510	2.53	2.38	3.1
Ethanol	0.09	433	4399	1.05	3.29	3.1
	0.11	425	3697	1.11	2.98	3.1
	0.13	417	3168	1.3	3.07	3.1
	0.16	426	2583	1.52	2.85	3.1
	0.19	435	2200	1.78	2.79	3.1
	0.22	454	1969	1.94	2.6	3.1
Isopropanol	0.09	419	4247	1.45	4.56	3.1
	0.11	422	3676	1.57	4.23	3.1
	0.13	426	3221	1.88	4.4	3.1
	0.16	441	2682	1.95	3.67	3.1
	0.19	460	2327	2.57	4.02	3.1
	0.22	474	2052	2.64	3.54	3.1
	0.25	489	1854	2.92	3.43	3.1
n-butanol	0.09	402	4061	1.51	4.72	3.1
	0.12	427	3719	1.74	4.39	3.1
	0.11	405	3523	1.64	4.42	3.1
	0.13	437	3319	1.87	4.36	3.1
	0.12	414	3139	1.83	4.3	3.1
	0.16	457	2781	2.26	4.26	3.1
	0.15	440	2675	2.15	4.35	3.1
	0.19	475	2396	2.69	4.21	3.1

range of ionization coefficient towards higher E/N values ($E/N > 3\,\mathrm{kTd}$). That range of E/N coincides with the conditions found in discharges for numerous applications.

The obtained results for effective ionization coefficients in vapours of different alcohols, together with the breakdown, and voltage-current measurements, provide a basis to produce complete sets of cross sections and other discharge parameters that can be used in plasma modeling. In case of ethanol and methanol data for other transport coefficients exist [46,47,51–54] while for the other two alcohols some additional information on cross sections or transport data may be required.

Acknowledgements The authors acknowledge support from the Serbian Ministry of Education, Science and Technological Development under project numbers OI 171037 and III 41011. Z. Lj. Petrović is grateful to the SANU project 155 and to Ulster University for support.

Author contributions

Jelena Marjanović—performed experimental measurements and calculations, analyzed the results, and wrote the draft of the manuscript. Dragana Marić—led the studies and interpretation of the results, participated in analysis, and discussion of the raw data and the results and participated in revising and writing the paper. Gordana Malović—helped in the analysis of measured data, participate in the discussion of the results, and in the editing of the manuscript. Zoran Lj. Petrović—defined the plan of research and design of experiment and development of the experimental procedure. He supervised the studies and analysis of the results, organization, and finalization of the manuscript.

Data Availability Statement This manuscript has no associated data or the data will not be deposited. [Authors' comment: This manuscript has all it's data presented in the Table 1 (in addition to figures).]

References

1. F. Chen, X. Huang, D. Cheng, X. Zhan, Int. J. Hydrogen Energy **39**(17), 9036–9046 (2014). https://doi.org/10.1016/j.ijhydene.2014.03.194
2. M.Z.F. Kamarudin, S.K. Kamarudin, M.S. Masdar, W.R.W. Daud, Int. J. Hydrogen Energy **38**, 9438 (2013). https://doi.org/10.1016/j.ijhydene.2012.07.059
3. P. Brunet, R. Rincón, J.M. Martinez, Z. Matouk, F. Fanelli, M. Chaker, F. Massines, Plasma Process. Polym. (2017). https://doi.org/10.1002/ppap.201700049
4. A. Ando, K. Ishikawa, H. Kondo, T. Tsutsumi, K. Takeda, T. Ohta, M. Ito, M. Hiramatsu, M. Sekine, M. Hori, Jpn. J. Appl. Phys. (2018). https://doi.org/10.7567/JJAP.57.026201
5. M. Matsushima, M. Noda, T. Yoshida, H. Kato, G. Kalita, T. Kizuki, H. Uchida, M. Umeno, K. Wakita, J. Appl. Phys. (2013). https://doi.org/10.1063/1.4794522
6. T. Hagino, H. Kondo, K. Ishikawa, H. Kano, M. Sekine, M. Hori, Appl. Phys. Express (2012). https://doi.org/10.1143/APEX.5.035101
7. I. Adamovich, S.D. Baalrud, A. Bogaerts, P.J. Bruggeman, M. Cappelli, V. Colombo, U. Czarnetzki, U. Ebert, J.G. Eden, P. Favia, D.B. Graves, S. Hamaguchi, G. Hieftje, M. Hori, I.D. Kaganovich, U. Kortshagen, M.J. Kushner, N.J. Mason, S. Mazouffre, S. Mededovic Thagard, H.-R. Metelmann, A. Mizuno, E. Moreau, A.B. Murphy, B.A. Niemira, G.S. Oehrlein, Z.Lj. Petrovic, L.C. Pitchford, Y.-K. Pu, S. Rauf, O. Sakai, S. Samukawa, S. Starikovskaia, J. Tennyson, K. Terashima, M.M. Turner, M.C.M. van de Sanden, A. Vardelle, J. Phys. D Appl. Phys. **50**, 323001 (2017). https://doi.org/10.1088/1361-6463/aa76f5
8. F. Fumagalli, O. Kylian, L. Amato, J. Hanus, F. Rossi, J. Phys. D Appl. Phys. (2012). https://doi.org/10.1088/0022-3727/45/13/135203
9. K.R. Stalder, G. Nersisyan, W.G. Graham, J. Phys. D Appl. Phys. **39**, 3457 (2006). https://doi.org/10.1088/0022-3727/39/16/S02
10. N. Puač, M. Gherardi, M. Shiratani, Plasma Process. Polym. (2018). https://doi.org/10.1002/ppap.201700174
11. N. Puač, S. Živković, N. Selaković, M. Milutinović, J. Boljević, G. Malović, Y.LJ. Petrović, Appl. Phys. Lett. **104**, 214106 (2014). https://doi.org/10.1063/1.4880360
12. P.J. Bruggeman, M. Kushner, B. Locke, H. Gardeniers, B. Graham, D. Graves, R. Hofman-Caris, D. Marić, J. Reid, E. Ceriani, D. Fernandez Rivas, J. Foster, S. Garrick, Y. Gorbanev, S. Hamaguchi, F. Iza, H. Jablonowski, E. Klimova, F. Krcma, J. Kolb, P. Lukes, Z. Machala, I. Marinov, D. Mariotti, S. Mededovic Thagard, D. Minakata, E. Neyts, J. Pawlat, Z.Lj. Petrović, R. Pflieger, S. Reuter, D. Schram, S. Schroeter, M. Shiraiwa, B. Tarabova, P. Tsai, J. Verlet, T. von Woedtke, K. Wilson, K. Yasui, G. Zvereva, Plasma Sources Sci. Technol. **25**, 053002 (2016). https://doi.org/10.1088/0963-0252/25/5/053002
13. A.V. Phelps, Rev. Mod. Phys. **40**, 399 (1968). https://doi.org/10.1103/RevModPhys.40.399
14. R.W. Crompton, Advances in atomic, molecular, and optical. Physics **33**, 97 (1994). https://doi.org/10.1016/S1049-250X(08)60034-8
15. R.W. Crompton, Aust. J. Phys. **25**(4), 409 (1972). https://doi.org/10.1071/PH720409
16. L.G.H. Huxley, R.W. Crompton, *The Diffusion and Drift of Electrons in Gases* (Wiley, New York, 1974)
17. R.D. White, M.J. Brunger, N.A. Garland, R.E. Robson, K.F. Ness, G. Garcia, J. de Urquijo, S. Dujko, Z.Lj. Petrović, Eur. Phys. J. D **68**, 125 (2014). https://doi.org/10.1140/epjd/e2014-50085-7
18. M.J.E. Casey, P.W. Stokes, D.G. Cocks, D. Bosnjaković, I. Simonović, M.J. Brunger, S. Dujko, Z.Lj. Petrović, R.E. Robson and R.D. White, Plasma Sources Sci. Technol. **30**, 035017 (2021). https://doi.org/10.1088/1361--6595/abe729
19. O. Šašić, S. Dupljanin, J. de Urquijo, Z.Lj. Petrović, J. Phys. D Appl. Phys. **46**, 325201 (2013). https://doi.org/10.1088/0022-3727/46/32/325201
20. L.J. Kieffer, JILA Information Center Report University of Colorado, Boulder, CO. USA 13 (1973)
21. L.G. Christophorou, S.R. Hunter, in *Electron Molecule Interactions and their Applications*, vol. 2, edited by L.G. Christophorou (Academic, New York, 1984), p. 317
22. S.R. Hunter, L.G. Christophorou, in *Electron Molecule Interactions and their Applications*, vol 2, edited by L.G. Christophorou (Academic, New York, 1984), p. 89
23. Y. Sakai, Appl. Surf. Sci. **192**, 327 (2002). https://doi.org/10.1016/S0169-4332(02)00034-X
24. R.D. White, R.E. Robson, M.A. Morrison, B. Li, K.F. Ness, J. Phys Conf. Ser. (2007). https://doi.org/10.1088/1742-6596/71/1/012004
25. R.L. Merlino, S.-H. Kim, J. Chem. Phys. (2008). https://doi.org/10.1063/1.3039078
26. Z.Lj. Petrović, S. Dujko, D. Marić, G. Malović, ŽNikitović, O. Šašić, J. Jovanović, V. Stojanović, M. Radmilović-Rađenović, J. Phys. D Appl. Phys. **42**, 194002 (2009). https://doi.org/10.1088/0022-3727/42/19/194002
27. R.E. Robson, Aust. J. Phys. **44**, 685 (1991). https://doi.org/10.1071/PH910685
28. A.V. Phelps, Z.Lj. Petrović, B.M. Jelenković, Phys. Rev. E **47**, 2825 (1993). https://doi.org/10.1103/PhysRevE.47.2825
29. J.S. Townsend, *The Theory of Ionization of Gases by Collision* (Constable, London, 1910)
30. A.V. Phelps, Z.Lj. Petrović, Plasma Sources Sci. Technol. **8**, 21 (1999). https://doi.org/10.1088/0963-0252/8/3/201

31. D. Marić, M. Savić, J. Sivoš, N. Škoro, M. Radmilović-Řadjenović, G. Malović, Z.Lj. Petrović, Eur. Phys. J. D **68**, 155 (2014). https://doi.org/10.1140/epjd/e2014-50090-x
32. J. Sivoš, D. Marić, N. Škoro, G. Malović, Z.Lj. Petrović, Plasma Sources Sci. Technol. **28**, 055011 (2019). https://doi.org/10.1088/1361-6595/ab0952
33. J. Sivoš, D. Marić, G. Malović, Z.Lj. Petrović, Eur. Phys. J. D **74**, 64 (2020). https://doi.org/10.1140/epjd/e2020-100540-3
34. D. Marić, G. Malović, Z.Lj. Petrović, Plasma Sources Sci. Technol. **18**, 034009 (2009). https://doi.org/10.1088/0963-0252/18/3/034009
35. G. Malović, A. Strinić, S. Živanov, D. Marić, Z.Lj. Petrović, Plasma Sources Sci. Technol. **12**, 1 (2003). https://doi.org/10.1088/0963-0252/12/4/399
36. R.C. Weast, *Handbook of Chemistry and Physics*, 51st edn. (Chemical Rubber Co, Cleveland, 1970)
37. Z.Lj. Petrović, A.V. Phelps, Phys. Rev. E **47**, 2806 (1993). https://doi.org/10.1103/PhysRevE.47.2806
38. N. Škoro, D. Marić, G. Malović, W.G. Graham, Z.Lj. Petrović, Phys. Rev. E **84**, 055401 (2011). https://doi.org/10.1103/PhysRevE.84.055401
39. Z.Lj. Petrović, A.V. Phelps, Phys. Rev. E **56**, 5920 (1997). https://doi.org/10.1103/PhysRevE.56.5920
40. R.W. Crompton, J. Dutton, S.C. Haydon, Nature **176**, 1079 (1955). https://doi.org/10.1038/1761079a0
41. M.M. Nikolić, A.R. Đorđević, I. Stefanović, S. Vrhovac, Z.Lj. Petrovic, IEEE Trans. Plasma Sci. **31**, 717 (2003) https://doi.org/10.1109/TPS.2003.815467
42. J. Sivoš, N. Škoro, D. Marić, G. Malović, Z.Lj. Petrović, J. Phys. D Appl. Phys. **48**, 424011 (2015). https://doi.org/10.1088/0022-3727/48/42/424011
43. T. Kuschel, I. Stefanović, G. Malović, D. Marić, Z.Lj. Petrović, Plasma Sources Sci. Technol. **22**, 045001 (2013). https://doi.org/10.1088/0963-0252/22/4/045001
44. B.M. Jelenković, A.V. Phelps, J. Appl. Phys. **85**, 7089 (1999). https://doi.org/10.1063/1.370516
45. B.M. Jelenković, A.V. Phelps, Phys. Rev. A **36**, 5310 (1987). https://doi.org/10.1103/PhysRevA.36.5310
46. H. Hasegawa, H. Date, J. Appl. Phys. (2015). https://doi.org/10.1063/1.4916606
47. H. Schlumbohm, Z. Angew. Physik **11**, 156 (1959)
48. H. Raether, Zeitschrift Für Physik **107**, 91 (1937). https://doi.org/10.1007/BF01330230
49. A. von Engel, *Ionized Gases* (Clarendon Press, Oxford, 1965), p. 325
50. D.M. Fadzillah, S.K. Kamarudin, M.A. Zainoodin, M.S. Masdar, Int. J. Hydrogen Energy **44**, 3031 (2019). https://doi.org/10.1016/j.ijhydene.2018.11.089
51. M.G. Curtis, l.C. Walker, J. Chem. Soc. Faraday Trans. **88**(19), 2805 (1992). https://doi.org/10.1039/FT9928802805
52. A. Peisert, F. Sauli, European Organization for Nuclear Research (CERN) Report No. CERN-84-08 **15**, 24 (1984)
53. M.J. Brunger, Int. Rev. Phys. Chem. **36**(2), 333 (2017). https://doi.org/10.1080/0144235X.2017.1301030
54. R. Rejoub, C.D. Morton, B.G. Lindsay, R.F. Stebbings, J. Chem. Phys. **118**, 1756 (2003). https://doi.org/10.1063/1.1531631

Eur. Phys. J. D (2024) 78:14
https://doi.org/10.1140/epjd/s10053-024-00808-8

THE EUROPEAN PHYSICAL JOURNAL D

Regular Article - Plasma Physics

Reduced ionization coefficients in low-current dc discharge in freons of a new generation

Jelena Marjanović[1,a], Dragana Marić[1], and Zoran Lj. Petrović[2,3]

[1] Institute of Physics, University of Belgrade, Pregrevica 118, 11080 Belgrade, Serbia
[2] Serbian Academy of Sciences and Arts, Knez Mihailova 35, 11001 Belgrade, Serbia
[3] School of Engineering, Ulster University, Jordanstown, Co. Antrim BT37 0QB, UK

Received 7 October 2023 / Accepted 23 January 2024 / Published online 4 February 2024

Abstract. In this paper we present results for reduced ionization coefficients (α/N, N—gas density) obtained from the breakdown voltage and emission profile measurements in low-pressure dc discharges in two freons: 1,1,1,2-tetrafluoroethane (R134a) with the chemical formula CH2F–CF3 and 2,3,3,3-tetrafluoropropene (HFO1234yf) with the chemical formula CH2=CFCF3. Our results for α/N are determined from the axial emission profiles in low-current Townsend discharge and lay in the intervals of reduced electric fields E/N (E—electric field, N—gas density), from 2.7 to 5.9 kTd for R134a and from 5 to 23 kTd for HFO1234yf. We also provide a comparison of our experimental results with those from the available literature.

1 Introduction

As technology continues to advance, energy consumption increases, which has a significant impact on environment. Numerous modern technologies still rely on the use of fluorocarbon gases, crucial for plasma etching processes that manufacture microchips and nanomaterials. Additionally, these gases are used in particle detection devices (RPC detectors), refrigeration systems, and gas filled electrical insulation [1, 2]. However, these gases have harmful effect on the environment, contributing to global warming and ozone depletion. In the past period, environmental protection has gained more attention globally, and scientists are actively seeking solutions to address pressing issues such as the greenhouse effect. As a result, there is a growing interest in exploring new gases with lower global warming potential (GWP) and lower ozone depletion potential (ODP), while also maintaining or enhancing the performance of gas discharge and cooling applications. As one of the first environmentally friendly fluorocarbons due to its low ozone depletion potential 1,1,1,2-tetrafluoroethane $C_2H_2F_4$ (CH2F–CF3) also known as R134a (or HFC134a), has recently been widely used in various applications. Due to its, still high global warming effect, this gas is slowly being phased out and replaced with newer, more effective alternatives. While this gas is being phased out there remains considerable interest in its cross sections as the application of gas discharges is one of the best methods to remediate the deleterious effects of HFC134a.

Hydrofluoroolefin $C_3H_2F_4$ (CH2=CFCF3) emerged as a promising alternative to replace 1,1,1,2-tetrafluoroethane primarily in numerous refrigerant applications due to its good characteristics and low GWP. The carbon–carbon double bond in $C_3H_2F_4$'s chemical structure makes it more reactive in the atmosphere, resulting in a lower GWP and shorter atmospheric lifetime compared to $C_2H_2F_4$. Additionally, this new type of freons is being viewed as a viable substitute for SF_6 in the latest technology of direct current underground transmission of medium and high-electric power using gas-insulated systems (DC GIS, DC GIL, DC bus systems).

For all applications involving gas discharges, it is necessary to carry out detailed studies on electrical characteristics, breakdown properties, electron transport coefficients, reaction rates, and more. In short, to ensure a smooth and proper functioning of those applications it is very important to obtain accurate and reliable data connected to elementary processes, atomic and molecular collisions of dominant particles, surface interactions, and breakdown conditions. Determining elementary electron–molecule collisions often involves fitting the calculated swarm parameters to experimental data [3–6]. Many applications operate at moderate and high electrical fields, making it crucial to gather data for those conditions. Pulsed Townsend experiments (PT) have simplified the process of obtaining and normalizing cross section data for moderate to high reduced

[a] e-mail: sivosj@ipb.ac.rs (corresponding author)

electrical fields E/N by utilizing drift velocities and ionization coefficients [7–10].

The breakdown condition is a highly sensitive projection of atomic and molecular collisions, as it depends on surface collisions of ions and atoms (and under some circumstances even photons and electrons). Our primary objective is to gather some of the elementary data on dc breakdown in low ODP and GWP fluorocarbon gases. We are researching the fundamental mechanisms that occur in these gases when they are exposed to electric fields. These mechanisms dictate the characteristics and behavior of breakdown and gas discharges and can offer valuable insights for modeling various gas discharge applications. In our measurements of breakdown and low-current regimes of dc discharges, we can determine coefficients for elementary processes of universal importance, such as ionization rate, secondary electron yield, and eventually the corresponding cross sections. In this paper, we will present the reduced ionization coefficients determined from the axial emission profiles of the low-current diffuse discharge regime (Steady State Townsend—SST) in gaseous 1,1,1,2-tetrafluoroethane (R134a, $C_2H_2F_4$) and its replacement gas, 2,3,3,3-tetrafluoropropene (HFO1234yf, $C_3H_2F_4$).

The spatial emission profiles are not merely a projection of the spatial profiles of the densities of particles, but also of their energy allowing them to excite the background molecules. The exponential growth of electrons toward the anode is expected, and unless the pressure is really low, these electrons may have enough space from their release as free particles to gain energy, come to equilibrium with the local field, and produce excitation. Simply speaking electrons gain energy fast and lose it only in inelastic collisions; while, elastic collisions are not efficient in distributing their kinetic energy. On the other hand, and as the basis for non-equilibrium plasmas, ions lose most of the kinetic energy in elastic collisions (momentum transfer). Hence, it takes them a longer space/time to reach the energies required for inelastic processes, i.e., excitation. As a matter of fact, under circumstances of discharges bordering with moderately high E/N, the ions do not have enough energy to perform excitation, much less ionization, so the emission profile will not project their spatial profile. According to Phelps and coworkers [11, 12], most of the heavy-particle excitation at such E/Ns is performed by fast neutrals. Ions are produced by electrons close to the anode and accelerate toward the cathode. In their wake fast neutrals are formed thus keeping the energy of ions relatively low (and limited). Therefore, the profile of fast neutrals' excitation (heavy particles) is almost constant after an increase close to the anode which is the result of both the growth of the number of ions with a superimposed equilibration distance. Spatial profiles due to combined effects of electrons, ions and fast neutrals have been modeled with high quantitative agreement with experiment [11–13]. One should note that in paper by Marić, Hartmann et al.[13] only the smallest E/N values correspond to those of this experiment. Still, with the same phenomenology and initial data excellent quantitative agreement is achieved for higher current glow discharges. Under such circumstances it is possible to isolate the electron induced excitation and thus to establish the ionization coefficient until heavy-particle excitation exceeds electron induced excitation significantly.

The use of ionization coefficient even in a limited range of E/N helps swarm analysis to fix the mean energies; while, drift velocities help establish momentum transfer. This may require additional information from the literature (such as ionization cross sections) but it may provide us with well-defined complete effective cross sections. Here 'effective' may mean that several processes may be coupled together into a single one, but that overall momentum and energy exchange together with particle number balance are defined and well established.

2 Experimental set-up

Breakdown measurements are carried out in a discharge chamber equipped with a plan-parallel electrode system [14, 15]. The electrode system is enclosed within a narrow cylinder made of quartz glass, which acts as a barrier to the long-path breakdown from electrodes to the metal components of the chamber (Fig. 1b). At the same time, it allows recording of side-on images of the discharge emission in a wide spectral range. The inter-electrode distance is adjustable and the present measurements were performed at the gap of 1.1 cm. The copper cathode and aluminum anode have a diameter of 5.4 cm. Figure 1a depicts a simplified schematic of the experimental set-up.

Before taking any measurements, the discharge chamber is evacuated by vacuum pumps until the pressure reaches around 10^{-6} Torr. Afterward, a high-current discharge of 30 μA is applied to the cathode surface in low-pressure hydrogen (around 1 Torr) for about 30 minutes. This is done until a stable operating voltage is achieved. The purpose of this treatment is to remove any oxide layers that may exist on the cathode surface, although it is impossible to completely remove stable oxide layers such as those found on materials like stainless steel, aluminum, and copper. However, this treatment can make them more uniform. Besides oxide removal, this process also eliminates any organic molecules and impurities from the cathode that might originate from pumping oils, resulting in a stable surface conditions that can be used for long periods of measurement. This procedure has been proven to provide reliable and reproducible breakdown data [17, 18]. To remove any impurities formed in the discharge chamber, both the treatment in the hydrogen discharge and measurements in selected freons are done in a slow flow regime.

Measurements were done for two freons: 1,1,1,2-tetrafluoroethane (R134a, $C_2H_2F_4$) and 2,3,3,3-tetrafluoropropene (HFO1234yf, $C_3H_2F_4$). The temperature in the laboratory was maintained at 21 °C

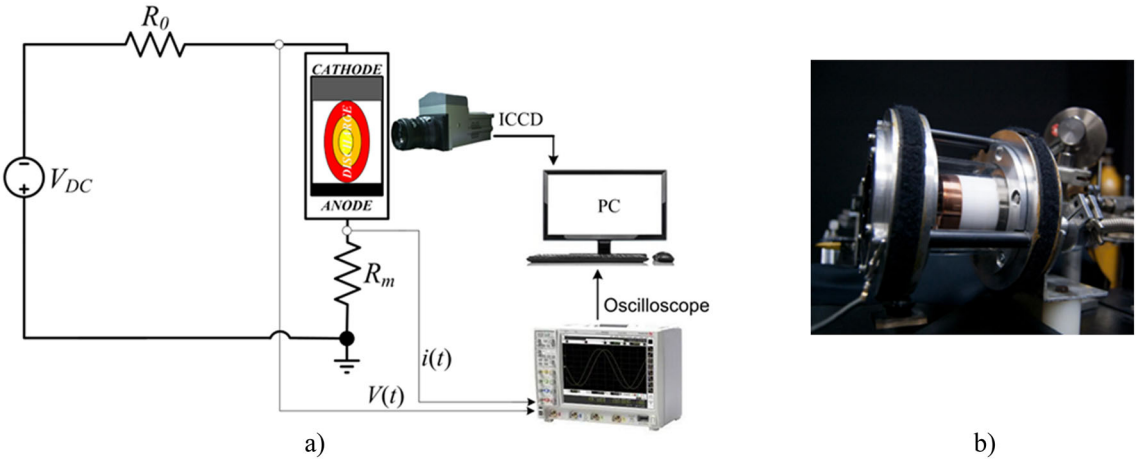

Fig. 1 **a** Schematics of the experimental set-up and the electrical circuit used in measurements. All the emission recordings were made with an ICCD camera. The series resistor R_0 is used to limit the current [16]; while, R_m is the "monitoring" resistor used to measure the discharge current; **b** photograph of the discharge chamber

using the air conditioning system. The electric circuit provided stable operation of the discharge in the low-current limit (near the breakdown conditions) [14, 18–20]. The critical elements of the external electric circuit are resistors R_0 and R_m (Fig. 1a). R_0 has a high resistance (˜MΩ) that limits the discharge current and keeps it in the range of the Townsend's regime. The resistor R_m is used to measure the discharge current, and it also strongly affects the oscillations of the current [16, 21]. A digital oscilloscope (Keysight Technologies DSO9104A) and two voltage probes (Tektronix P6915 and Agilent 10076A) are used for the detection of electrical signals.

The discharge chamber design (Fig. 1b) enables side-on recordings of emission intensity along the longitudinal chamber axis. To capture light emission, we used a sensitive ICCD camera (Andor IStar DH720-18U-03) equipped with a glass lens (Nikkor 50 mm f/1.4D) and a UV lens (Nikon UV-105, 105 mm f/4.5) that allows us to acquire axial discharge profiles of spectrally integrated emission in the near UV and visible range of the spectrum, defined by the transparency of the lenses and the quantum efficiency of the ICCD photocathode. However, the total emission profiles of the discharge (obtained by integrating the emission in the whole visible range) did not reflect the electron excitation well for the freons studied in this work. They included significant emission from heavy particle induced excitation processes. We used optical filters to get the emission profiles that we needed for the determination of the ionization coefficients. By adding band-pass optical filters, we recorded profiles associated with specific spectral lines (Hα at 656 nm and CH at 314 nm and 431 nm) that provided us with additional information on particular processes of excitation [15, 19]. These emission profiles show only a small contribution of fast neutrals and ions to excitation [15], enabling us to extend the range of measurement of ionization coefficients to somewhat higher E/N.

In addition to ionization coefficients that only require relative spatial profiles, the presently determined data allow us to fit the absolutely normalized axial profiles of emission and thus establish cross sections for the heavy-particle excitation of these molecules [12, 22]. As such a study requires a lot of additional data that may not be available, it is beyond the scope of the present paper.

3 Results and discussion

Self-sustained discharges operating in the low-current limit (no space charge, constant electric field) can be used to determine exactly the ionization coefficients. Such conditions can be accomplished in Steady State Townsend (SST) experiments that operate close to the breakdown conditions. Namely, in the initial phase of breakdown, electron multiplication is determined by the external electric field only. The expanding space charge has been utilized as a disturbance to the distribution of the external field to develop an exact model of low-current discharges [17, 21]. We can now distinguish conditions where space charge effects are negligible by recording the Volt-Ampere characteristics and spatial profiles of the discharge emission [15, 19, 23].

The total emission profiles recorded over the entire range of reduced electric fields covered by the Paschen curve recording for both R134a and HFO1234yf are not suitable to determine α/N (see the example of recorded total profile (black line) around the Paschen minimum for R134a in Fig. 2). This is because the emission in front of the cathode from the heavy-particle excitation masks the part of the profile related to electron-induced ionization and excitation [11, 13, 24]. The spectrally resolved measurements by using band-pass optical filters enable us to obtain the Hα emission profiles (at 656 nm) and CH emission profiles (at 314 nm and

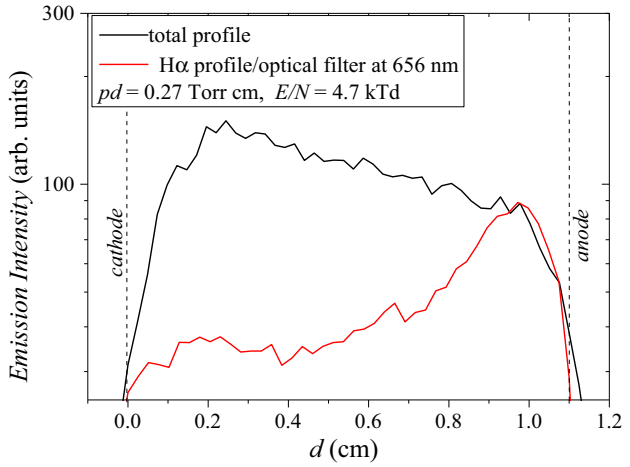

Fig. 2 Example of the experimentally recorded axial emission profiles in low-current Townsend discharge in R134a gas at $pd = 0.27$ Torr cm, $V_b = 428$ V, and $E/N = 4.7$ kTd at electrode distance of $d = 1.1$ cm: (black line)—total emission profile recorded in whole visual range, (red line)—Hα emission profile recorded with optical filter at 656 nm. The profile obtained at 656 nm is normalized to the maximum emission intensity in front of the anode of the total profile

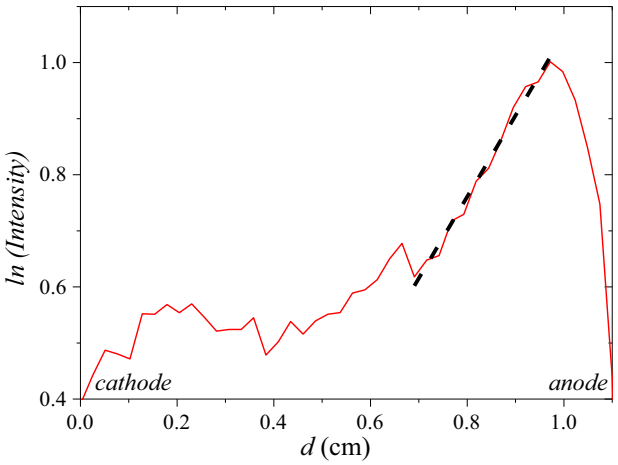

Fig. 3 Hα axial emission profile in low-current Townsend discharge in R134a gas at $pd = 0.27$ Torr cm, $V_b = 428$ V, and $E/N = 4.7$ kTd at electrode distance of $d = 1.1$ cm. The plot of the emission profile in the semi-log scale reflects electron multiplication between the electrodes, and the profile slope (black line) corresponds to the ionization coefficient

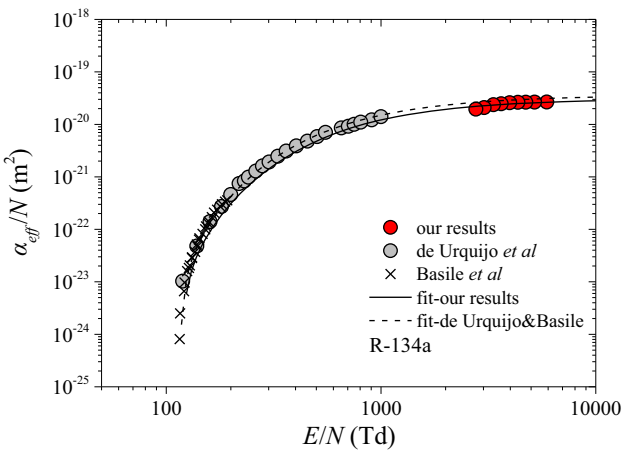

Fig. 4 Dependence of reduced effective ionization coefficient (α_{eff}/N) on reduced electric field (E/N) in R134a. Results obtained from our experiment (red circles) are compared with data for R134a from de Urquijo et al. (gray circles) [29] and Basile et al.(black X) [30]

431 nm) (Fig. 2 and Fig. 5). The emission of CH radicals comes from two systems: the $C^2\Sigma^+ \rightarrow X^2\Pi$ system with the band-head at 314 nm and the $A^2\Delta^+ \rightarrow X^2\Pi$ system with the band-head at 431 nm [25, 26]. The emission profiles of Hα (red line in Figs. 2 and 5) and CH at 314 nm (blue line in Fig. 5) show dominant emission, i.e., exponential growth toward the anode produced mainly by electron excitation.

Experimentally recorded emission profiles with band-pass optical filter at 656 nm for the low-current limit of the dc discharges in the Townsend/diffuse regime in R134a proved to be sufficiently good to obtain the ionization coefficient for this gas as heavy-particle excitation for this line and this gas was negligible below the E/N of 5.9 kTd. Figure 3 shows an example of an experimentally recorded Hα emission profile in low-current Townsend discharge in R134a. Exponential growth is best observed if plotted in a semi-logarithmic scale where the slope corresponds to the ionization coefficient α/N (Fig. 3), once equilibrium with the local field is reached [18, 23, 27, 28].

Figure 4 also shows the dependence of the effective ionization coefficients α_{eff}/N on reduced electric field E/N from the literature [29, 30] and our experiment for the discharge in R134a. Our results for α/N are obtained from Hα emission profiles and cover the range of E/N from 2.7 to 5.9 kTd (red circles in Fig. 4). The upper limit is determined by the increasing contribution of the fast neutrals making separation of electron and fast neutral induced emission profiles impossible. The lower limit is determined by unstable operation of the Townsend discharge whereby it is not possible to use oscillating discharges to determine precise spatial emission profiles. De Urquijo's [29] and Basile's [30] results for R134a cover the region of much lower values of the reduced electric fields from 120 Td to 1 kTd, and the agreement between these two sets of data is very good.

In Fig. 4 we also show two fitting curves to our experimental data and the data compiled of de Urquijo et al. [29] and Basile et al. [30]. Fits are obtained by using the extended Townsend's formula, a semi-empirical formula proposed by Phelps and Petrović [17, 20] and additionally evaluated for several gases in [31]. The extended Townsend's formula represents a sum of several terms identical to the Townsend's formula for ionization coefficient, but the values of parameters are different. Physical meaning for using the multi-term formula can be

Table 1 Coefficients of the Townsend formula fit in the E/N range 120 Td–5.9 kTd for R134a

Formula $\frac{\alpha}{N} = \sum_{i=0}^{2} A_i \exp\left(\frac{-B_i}{\frac{E}{N}}\right)$	Range (Td)	A_0 (V m)	B_0	A_1 (V m)	B_1	A_2 (V m)	B_2
Our results	2700–5900	7×10^{-21}	750	2.4×10^{-20}	1000	-1.996×10^{-23}	10
de Urquijo et al. [29]	120–1000	5.2×10^{-21}	790	3.1×10^{-20}	900	-1.98×10^{-23}	1

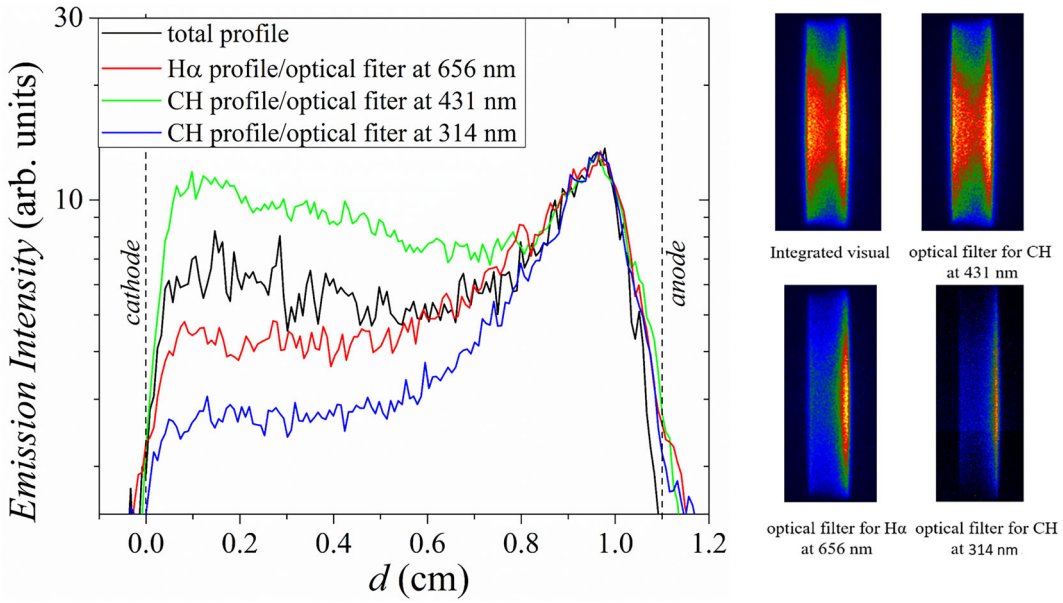

Fig. 5 Example of the experimentally recorded 2D images and axial emission profiles in low-current Townsend discharge in HFO1234yf gas at $pd = 0.25$ Torr cm, $V_b = 644$ V, and $E/N = 7.8$ kTd at electrode distance of $d = 1.1$ cm: (black line)—total emission profile recorded in whole visual range, (red line)—Hα emission profile recorded with optical filter at 656 nm, (green line)–CH emission profile recorded with optical filter at 431 nm, (blue line)—CH emission profile recorded with optical filter at 314 nm. The profiles obtained by optical filters are normalized to the maximum emission intensity of the total profile

found in the existence of several different groups of electrons in the discharge, with the coefficient B_i showing the E/N range where the term i is significant and A_i giving the maximal contribution of the term [31]. Moreover, the dominant term in the multi-term formula should be similar to the standard Townsend single term formula fit for the same gas. Coefficients obtained by fitting the experimental data by the 3-term analytical formula are given in Table 1. In the table we also provide the E/N region where the fits are valid. It should be noted that the negative A_i coefficient in the formula allows adjustment of the fit to represent decreasing of α/N with E/N due to a decrease of the ionization cross section at higher electron energies [31]. Fitting coefficients obtained for the present experimental results are valid for our measurement range (2.7–5.9 kTd). They also agree with de Urquijo and Basile's data in the lower E/N range so the range of validity may be extended down to 120 Td.

In the case of 2,3,3,3-tetrafluoropropene (HFO1234yf), we were able to determine the ionization coefficients from two different axial emission profiles in a low-current Townsend discharge recorded with band-pass optical filters at 314 nm (CH emission profiles) and 656 nm (Hα emission profiles). Figure 5 shows an example of axial emission profiles recorded with and without optical filters at 7.8 kTd and the differences in their shape, due to the contribution of excitation by heavy particles (fast neutrals, ions) and electrons. The ionization coefficients resulting from the CH emission profile (blue line in Fig. 5) and from the Hα emission profile (red line in Fig. 5) are practically identical, despite using two different lines. However, with an increase of reduced electric field (E/N), the contribution of heavy particles increases first for Hα, and it overlaps with the exponential growth of electrons dominated excitation. Thus, at higher E/N we begin to obtain very different exponential slopes toward the anode (Fig. 6). We found that up to around 8 kTd, the ionization rates obtained from Hα and 314 nm CH profiles were in reasonable agreement. For higher E/N (e.g., 9 kTd and more, as shown in Figure 6), the spatial profile for Hα (red line in Fig. 6) is drowned by the fast neutral excitation and the resulting ionization coefficients begin to deviate considerably from those obtained from the CH spatial profile (blue line in Fig. 6). As a result, the Hα spatial profile does not have an observable separation of fast

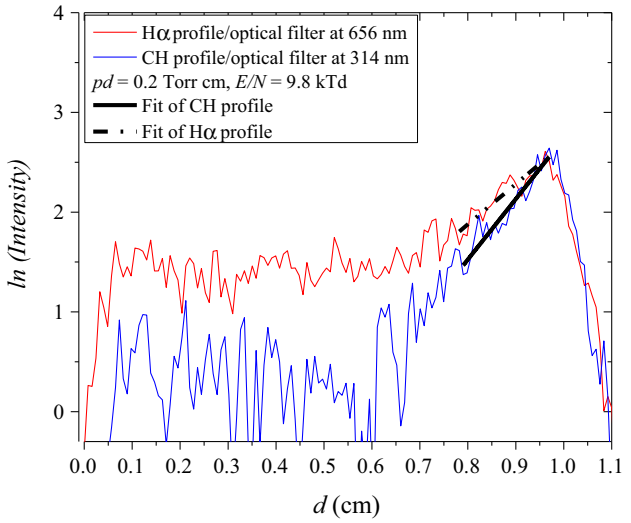

Fig. 6 Hα and CH axial emission profiles in low-current Townsend discharge in HFO1234yf gas at $pd = 0.2$ Torr cm and $E/N = 9.8$ kTd at electrode distance of $d = 1.1$ cm. The profiles slope (black solid and dash-dot lines) corresponds to the ionization coefficient

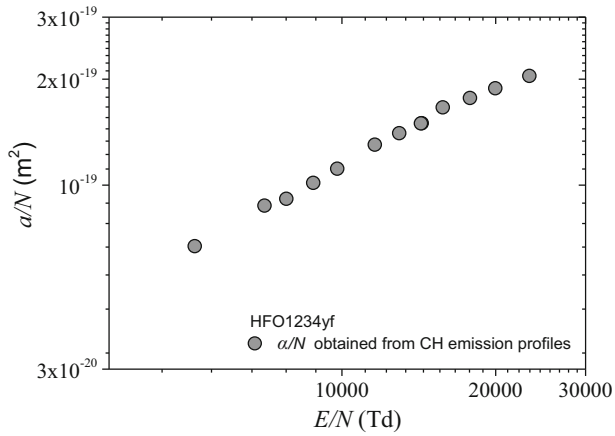

Fig. 7 Dependence of reduced ionization coefficient (α/N) on the reduced electric field (E/N) in HFO1234yf discharge obtained from CH axial emission profiles recorded using optical filter at 314 nm

neutral and electron excitation. Therefore, we chose to use the ionization coefficients obtained from the CH emission profiles at 314 nm above 5 kTd and up to 23 kTd. Beyond the latter E/N, again, we could not separate the contributions of electrons and fast neutrals to the excitation this time of the CH band. The dependence of the ionization coefficient α/N for 2,3,3,3-tetrafluoropropene (HFO1234yf) on the reduced electric field E/N is shown in Figure 7.

The results for reduced ionization coefficient presented in Fig. 7 cover a relatively high range of reduced electric fields from 5 to 23 kTd. These α/N values correspond to excitation emission of CH in collision with electrons, and evidence of that is the exponential increase of emission intensity toward the anode presented by example of CH emission profile (Fig. 5). Additionally, we give numerical data listed in Table 2 that correspond to the results shown in Figs. 4 and 7.

4 Conclusion

Non-equilibrium discharges in fluorocarbons, especially those that belong to the new generation, are important research topics because of their wide applications. To achieve new and better applications or to address the global pollution of the atmosphere, we require data, a thorough understanding, and insights into elementary processes. These are all essential for modeling gas plasmas, which can offer the best opportunity to reduce pollutant densities. Therefore, we present the results for ionization coefficients from our experimental study of low-pressure dc breakdown in 1,1,1,2-tetrafluoroethane (R134a, $C_2H_2F_4$) and its lower GWP substitute gas, 2,3,3,3-tetrafluoropropene (HFO1234yf, $C_3H_2F_4$). We obtained ionization coefficients from axial emission profiles in low-current Townsend discharges under conditions with dominant electron excitation of the background gas (high pressure i.e., lower E/N). Our results cover the reduced electric field ranges: 2.7–5.9 kTd for R134a and 5–23 kTd for HFO1234yf. There is little or no data in the literature on ionization coefficients for discharges in different HFOs.

For R134a, we were able to compare our results with those from the literature. Our results agree reasonably well with the experimental measurements of de Urquijo et al. [29] and Basile et al. [30], although the E/N ranges do not overlap. We could not get results for α/N for lower E/N values ($E/N < 2.7$ kTd) because of the limitations of the experiment and the electrical circuit components that prevented us from having a stable dc dark Townsend discharge (i.e., without oscillations) [20]. However, our measurements allowed us to extend the ionization coefficient range to higher E/N values ($E/N > 2$ kTd), which are relevant for many applications. The results for ionization coefficients along with the breakdown and voltage–current measurements, by giving a better handle on the mean energy allow development of complete sets of cross sections and other discharge parameters in the mean energy region relevant for plasma modeling.

Table 2 Ionization coefficients obtained in our experimental measurements of discharges in freons R134a and HFO1234yf

	p (Torr)	V_b (V)	E/N (Td)	α/N 10^{-20} (m^2)
R134a	0.2	432	5913	2.67
from Hα emission profiles	0.23	428	5189	2.65
	0.25	428	4722	2.64
	0.27	429	4342	2.62
	0.3	432	3972	2.58
	0.33	436	3628	2.47
	0.36	440	3339	2.37
	0.41	448	3021	2.1
	0.45	456	2767	1.94
HFO1234yf				
from CH emission profiles				
	0.09	764	23,285	20.42
	0.1	724	19,970	18.84
	0.11	704	17,814	17.68
	0.12	680	15,761	16.62
	0.13	673	14,334	14.99
	0.14	662	12,950	14.04
	0.16	654	11,600	13.03
	0.18	648	9793	11.13
	0.2	642	8788	10.15
	0.23	642	7783	9.14
	0.25	642	7054	8.74
	0.35	660	5149	6.71

During the measurements, the room temperature was $T = 21$ °C and electrode gap was $d = 1.1$ cm

Acknowledgements The authors acknowledge support from the Serbian Ministry of Science and Technological Development and Innovation. This research was supported by the Science Fund of the Republic of Serbia, Grant No. 7749560, project EGWIn. Zoran Lj. Petrović is grateful to the SASA project F155.

Author contributions

JM performed experimental measurements and calculations, analyzed the results, and wrote the draft of the manuscript. DM led the studies and interpretation of the results, participated in analysis and discussion of the raw data and the results, and participated in revising and writing the paper. ZLP defined the plan of research and design of experiment and development of the experimental procedure. He supervised the studies and analysis of the results, organization, and finalization of the manuscript.

Data Availability Statement This manuscript has no associated data, or the data will not be deposited. [Authors' comment: This manuscript has all its data presented in the Tables 1 and 2 (in addition to figures)].

References

1. A. Bianchi, S. Delsanto, P. Dupieux, A. Ferretti, M. Gagliardi, B. Joly, S.P. Manen, M. Marchisone, L. Micheletti, A. Rosano, E. Vercellin, JINST **14**, P1101414 (2019). https://doi.org/10.1088/1748-0221/14/11/P11014
2. M. Koch, C.M. Franck, IEEE Trans. Dielectr. Electr. Insul. **22**(6), 3260 (2015). https://doi.org/10.1109/TDEI.2015.005118
3. A.V. Phelps, Rev. Mod. Phys. **40**, 399 (1968). https://doi.org/10.1103/RevModPhys.40.399
4. R.W. Crompton, Adv. At. Mol. Opt. Phys. **33**, 97 (1994). https://doi.org/10.1016/S1049-250X(08)60034-8
5. R.W. Crompton, Aust. J. Phys. **25**(4), 409 (1972). https://doi.org/10.1071/PH720409
6. L.G.H. Huxley, R.W. Crompton, *The Diffusion and Drift of Electrons in Gases* (Wiley, New York, 1974)
7. Z.L. Petrović, M. Šuvakov, Ž Nikitović, S. Dujko, O. Šašić, J. Jovanović, G. Malović, V. Stojanović, Plasma Sources Sci. Technol. **16**, S1–S12 (2007). https://doi.org/10.1088/0963-0252/16/1/S01
8. Z.L. Petrović, S. Dujko, D. Marić, G. Malović, Ž Nikitović, O. Šašić, J. Jovanović, V. Stojanović, M. Radmilović-Radenović, J. Phys. D Appl. Phys. **42**,

194002 (2009). https://doi.org/10.1088/0022-3727/42/19/194002
9. R.D. White, M.J. Brunger, N.A. Garland, R.E. Robson, K.F. Ness, G. Garcia, J. de Urquijo, S. Dujko, Z.L. Petrović, Eur. Phys. J. D **68**, 125 (2014). https://doi.org/10.1140/epjd/e2014-50085-7
10. M.J.E. Casey, P.W. Stokes, D.G. Cocks, D. Bosnjaković, I. Simonović, M.J. Brunger, S. Dujko, Z.L. Petrović, R.E. Robson, R.D. White, Plasma Sources Sci. Technol. **30**, 035017 (2021). https://doi.org/10.1088/1361-6595/abe729
11. B.M. Jelenković, A.V. Phelps, Phys. Rev. A **36**, 5310 (1987). https://doi.org/10.1103/PhysRevA.36.5310
12. Z.L. Petrović, A.V. Phelps, Phys. Rev. E **80**, 016408 (2009). https://doi.org/10.1103/PhysRevE.80.016408
13. D. Marić, P. Hartmann, G. Malović, Z. Donko, Z.L. Petrović, J. Phys. D Appl. Phys. **36**, 2639 (2003). https://doi.org/10.1088/0022-3727/36/21/007
14. D. Marić, G. Malović, Z.L. Petrović, Plasma Sources Sci. Technol. **18**, 034009 (2009). https://doi.org/10.1088/0963-0252/18/3/034009
15. J. Sivoš, D. Marić, G. Malović, Z.L. Petrović, Eur. Phys. J. D **74**, 64 (2020). https://doi.org/10.1140/epjd/e2020-100540-3
16. Z.L. Petrović, A.V. Phelps, Phys. Rev. E **47**, 2806 (1993). https://doi.org/10.1103/PhysRevE.47.2806
17. A.V. Phelps, Z.L. Petrović, Plasma Sources Sci. Technol. **8**, 21 (1999). https://doi.org/10.1088/0963-0252/8/3/201
18. D. Marić, M. Savić, J. Sivoš, N. Škoro, M. Radmilović-Řadjenović, G. Malović, Z.L. Petrović, Eur. Phys. J. D **68**, 155 (2014). https://doi.org/10.1140/epjd/e2014-50090-x
19. J. Sivoš, D. Marić, N. Škoro, G. Malović, Z.L. Petrović, Plasma Sources Sci. Technol. **28**, 055011 (2019). https://doi.org/10.1088/1361-6595/ab0952
20. Z.L. Petrović, A.V. Phelps, Phys. Rev. E **56**, 5920 (1997). https://doi.org/10.1103/PhysRevE.56.5920
21. A.V. Phelps, Z.L. Petrović, B.M. Jelenković, Phys. Rev. E **47**, 2825 (1993). https://doi.org/10.1103/PhysRevE.47.2825
22. V.D. Stojanović, B.M. Jelenković, Z.L. Petrović, J. Appl. Phys. **81**, 1601 (1997). https://doi.org/10.1063/1.364089
23. J. Marjanović, D. Marić, G. Malović, Z.L. Petrović, Eur. Phys. J. D **75**, 191 (2021). https://doi.org/10.1140/epjd/s10053-021-00138-z
24. B.M. Jelenković, A.V. Phelps, J. Appl. Phys. **85**, 7089 (1999). https://doi.org/10.1063/1.370516
25. A.G. Gaydon, *The Spectroscopy of Flames*, 2nd edn. (Chapman and Hall, London, 1974)
26. R.A. Durie, Proc. Phys. Soc. A **65**, 125 (1952). https://doi.org/10.1088/0370-1298/65/2/307
27. G. Malović, A. Strinić, S. Živanov, D. Marić, Z.L. Petrović, Plasma Sources Sci. Technol. **12**, 1 (2003). https://doi.org/10.1088/0963-0252/12/4/399
28. T. Kuschel, I. Stefanović, G. Malović, D. Marić, Z.L. Petrović, Plasma Sources Sci. Technol. **22**, 045001 (2013). https://doi.org/10.1088/0963-0252/22/4/045001
29. J. de Urquijo, A. Juárez, E. Basurto, J.L. Hernández-Ávila, Eur. Phys. J. D **51**, 241 (2009). https://doi.org/10.1140/epjd/e2008-00288-6
30. G. Basile, I. Gallimberti, S. Stangherlin, T.H. Teich, in *Proceedings of the XX Interenational Conference on Phenomena in Ionized Gases*, ed. by M. Vaselli, vol 2 (1991), p. 361
31. D. Marić, M. Radmilović-Radenović, Z.L. Petrović, Eur. Phys. J. D **35**, 313 (2005). https://doi.org/10.1140/epjd/e2005-00172-y